AGU100 ADVANCING EARTH AND SPACE SCIENCE

Water Resources Research

RESEARCH ARTICLE
10.1029/2017WR021964

Time-Varying Storage–Water Age Relationships in a Catchment With a Mediterranean Climate

Nicolas B. Rodriguez[1,2], Kevin J. McGuire[3], and Julian Klaus[1]

[1]Catchment and Eco-Hydrology Research Group, Environmental Research and Innovation Department, Luxembourg Institute of Science and Technology, Belvaux, Luxembourg, [2]Institute of Water Resources and River Basin Management, Karlsruhe Institute of Technology, Karlsruhe, Germany, [3]Virginia Water Resources Research Center and Department of Forest Resources and Environmental Conservation, Virginia Tech, Blacksburg, VA, USA

Key Points:
- Storage-water age relationships generally correspond to the inverse storage effect in a catchment exposed to a Mediterranean climate
- The marked seasonal climate at this study site caused short-term deviations from the inverse storage effect
- Streamflow SAS functions were a consistent lumped description of rainfall-runoff processes

Correspondence to:
N. Rodriguez,
nicolas.rodriguez@list.lu

Citation:
Rodriguez, N. B., McGuire, K. J., & Klaus, J. (2018). Time-varying storage–Water age relationships in a catchment with a Mediterranean climate. *Water Resources Research*, *54*, 3988–4008. https://doi.org/10.1029/2017WR021964

Received 28 SEP 2017
Accepted 23 APR 2018
Accepted article online 27 APR 2018
Published online 27 JUN 2018

Abstract Recent studies on the relationships between catchment storage and water ages using Travel Time Distributions (TTDs), Residence Time Distributions (RTDs), and StorAge Selection (SAS) functions have led to the hypothesis that streamflow preferentially mobilizes younger water when catchment storage is high. This so-called "Inverse Storage Effect" (ISE) needs further evaluation in more catchments with diverse climates and physiographical features. In this work, we assessed the validity of the ISE in WS10 (H. J. Andrews forest, Oregon, USA), a forested headwater catchment in a Mediterranean climate. A conceptual model of the catchment, developed based on experimental observations of water flow paths in WS10, was calibrated to streamflow and $\delta^{18}O$ in streamflow. Based on the calibrated model results, we determined RTDs, and streamflow TTDs and SAS functions by assuming that the soil reservoir and the groundwater reservoir act as well-mixed systems. The streamflow SAS functions and travel time dynamics showed that the ISE generally applies in WS10. Yet, during transitions from dry summer periods to wet winter periods and vice versa, the marked seasonal climate caused rapid and strong storage variations in the catchment, which led to deviations from the ISE. The seasonality of streamflow travel times in WS10 is the result of the seasonal contributions of younger water from the hillslopes added to the rather constant groundwater contributions of older water. The streamflow SAS functions were able to capture the relative importance of contrasting flow paths in the soils and in the bedrock highlighted by previous studies in WS10.

Plain Language Summary Water age, which is the time water spends in a catchment after entering it, is a fundamental descriptor of how water flows through catchments. Recently, it was hypothesized that in many catchments, streamflow is fed by the youngest water present in the catchment when it is wet. In this work, we determined how the water of various ages feeds streamflow in the catchment WS10 (H. J. Andrews forest, Oregon, USA), a forested headwater catchment in a Mediterranean climate. A model of the catchment WS10 was used to simulate streamflow and water isotopic composition (i.e., oxygen-18, ^{18}O) as a tracer, which is naturally present in precipitation. Once calibrated to the observed data, the model allowed an examination of the water ages in the catchment and in streamflow. The model results revealed that in WS10, streamflow is also fed by the youngest water during wetter times of the year. However, during transition periods when the catchment is wetting up or drying out, more complex combinations of water ages contribute to streamflow because of the marked climate seasonality. Our findings imply that the relationships between catchment wetness and water ages need to be regarded as time-variant in catchments exposed to a Mediterranean climate.

1. Introduction

The chemical composition of water in catchment storage and discharge is largely governed by the contact times between water and catchment material, i.e., by the age of water. The distributions of water ages in catchment storage (residence time distributions, RTDs) and in catchment outflows (travel time distributions, TTDs) have been used previously to describe how catchments store and release water and solutes (Benettin et al., 2015a, 2017; Godsey et al., 2010; Hrachowitz et al., 2016; Kirchner et al., 2000; Maher, 2010, 2011; McGuire & McDonnell, 2006; Rinaldo & Marani, 1987; van der Velde et al., 2012). A recent study gathered

stable isotope tracer data from 254 catchments and suggested that, on a global scale, about a third of the streamflow volume consists of young water from recent precipitation (Jasechko et al., 2016). In contrast, the remaining two-thirds of the streamflow volume comes from much older water mobilized from catchment storage (Jasechko et al., 2016). Streamflow TTDs and catchment RTDs appear to be very different, which shows that streamflow is not a uniform mixture of all the water stored in a catchment, but represents only a fraction of the storage at any time. This perception is supported by detailed investigations of tracer transport in catchments using lumped conceptual models (e.g., Birkel et al., 2011b; Fenicia et al., 2010; Hrachowitz et al., 2013, 2015; McMillan et al., 2012). In these studies, mixing coefficients were used within conceptual control volumes to represent how incoming rainfall mixes with the stored water and is eventually released by outflows. This suggested that a complete mixing of the entire catchment volume is inadequate to simulate tracer concentrations of outflows in many catchments. Furthermore, these studies showed that catchment TTDs and RTDs are highly time-variant.

Other recent work used StorAge Selection (SAS) functions, defined as the ratio of TTD and RTD, for relating water ages in storage and outflows without assuming stationarity (Benettin et al., 2015c; Botter, 2012; Botter et al., 2011; Rinaldo et al., 2015; van der Velde et al., 2012). SAS functions are a lumped characterization of the mixing of various water ages in storage when they are released as discharge or evapotranspiration. Thus, SAS functions provide a theoretically consistent lumped description of water and solute transport in catchments, in which TTDs and RTDs are allowed to differ from each other and vary individually in time (Rinaldo et al., 2015). Therefore, SAS functions are seen as a promising tool to better understand the complexity of streamflow generation processes, calculate time-varying TTDs and RTDs, and simulate water and solute transport in catchments (Benettin et al., 2015a, 2017; Harman, 2015; van der Velde et al., 2015).

Studies with SAS functions in catchments with strong oceanic climates, e.g., in the Upper Hafren catchment in Wales (Benettin et al., 2015b; Harman, 2015), and in the Bruntland Burn catchment in Scotland (Benettin et al., 2017), supported the emerging perception that younger water stored in the catchments is preferentially mobilized to generate streamflow when catchment storage is high. This was termed "Inverse Storage Effect" (ISE) by Harman (2015). The ISE was also shown to be relevant in a laboratory-scale experiment, where breakthrough curves of irrigation water tagged with different tracers on a sloping lysimeter were used to examine transport processes (Kim et al., 2016). SAS functions, calculated from tracking virtual particles with a physically based model of the same sloping lysimeter, showed a similar dependence on the system wetness (Pangle et al., 2017) to what was found in the Upper Hafren and the Bruntland Burn catchments. Other studies have shown that streamflow travel times tend to decrease for wetter catchment states, which points to an ISE-like behavior (Botter et al., 2010; Heidbüchel et al., 2012; Hrachowitz et al., 2013, 2015; Klaus et al., 2015; Rinaldo et al., 2011; Segura et al., 2012; Soulsby et al., 2015a; van der Velde et al., 2015). Until now, the ISE phenomenon has been observed mostly in systems with limited seasonality for precipitation, evapotranspiration, and streamflow, and where evapotranspiration is rather low. Calculating time-varying streamflow SAS functions and travel times in catchments with diverse climates and physiographical features is essential for determining the generality of the ISE.

Physically based particle tracking approaches recently estimated nonparametric SAS functions and linked them to flow paths on small scale (Pangle et al., 2017) and in virtual media (Danesh-Yazdi et al., 2018). Yet, catchment scale approaches for tracer transport and travel time estimates commonly rely on lumped representations based on parameterized SAS functions. At the catchment scale, SAS functions are usually assumed to be distinct functions of one-to-three parameters calibrated with tracer data (e.g., gamma, beta, and power law functions) (cf. Rinaldo et al., 2015). To be meaningful, this assumption of the shape of SAS functions and their parameters needs to be compared to observed runoff generation and solute transport processes in catchments. Establishing a clearer link between time-varying SAS functions and travel times at the catchment scale, and observed physical processes will help hydrologists develop and justify lumped modeling approaches based on travel times. This is particularly important since lumped catchment models that employ time-varying travel times are seen as a unifying modeling framework for the currently separate catchment hydrology and water quality scientific communities (Hrachowitz et al., 2016). Well-researched experimental catchments provide the opportunity to link travel time theory to hydrological processes.

In this study, we designed and calibrated a conceptual catchment flow and transport model that allowed us to solve the Master Equation (Botter et al., 2011) and derive time-varying RTDs, and streamflow TTDs and SAS functions in the well-studied catchment WS10 in the H. J. Andrews Experimental Forest in Oregon, USA.

We assumed that the modeled soil reservoir and groundwater reservoir act as well-mixed systems. The novelty of this work lies in the pronounced seasonality of the Mediterranean climate of the study site allowing the direct examination of the ISE. Moreover, the large number of previous studies on rainfall-runoff in WS10 allows a benchmarking of streamflow SAS functions against physical processes in the catchment. The present study aims to shed light on the following research questions:

1. Is the inverse storage effect a characteristic feature in the Mediterranean climate?
2. Are time-varying streamflow SAS functions and travel times consistent with previous detailed investigations of flow paths in an experimental catchment?

2. Materials and Methods

2.1. Study Site

This study is carried out in WS10, a forested headwater catchment (10.2 ha) located in the H. J. Andrews forest (HJA) in the central Western Cascades of Oregon, USA (44.2°N, 122.25°W) (Figure 1). The climate is Mediterranean, with a strong contrast between the dry summers and the wet winters (Greenland, 1994). Annual precipitation averages 2,200 mm (1990–2003), with 80% of precipitation falling predominantly as rainfall between October and April. Minor snow accumulation ($<$ 30 cm) is not uncommon in winter at WS10, but it rarely lasts longer than a few weeks, and on average melts within a few days (Harr & McCorison, 1979; Sollins & McCorison, 1981). During the isotopic sampling for this study, no major snow accumulation was observed in WS10 (McGuire et al., 2007; McGuire & McDonnell, 2010). We therefore neglected snow processes for the purpose of this study, consistent with previous studies using the same data set (Klaus et al., 2015; McGuire et al., 2005, 2007). The mean annual runoff ratio in WS10 is 0.60 over February 2001–2003. Evapotranspiration varies seasonally between less than 1 mm/d in winter and 5 mm/d in summer (Barnard et al., 2010; McGuire et al., 2007). This creates a distinct seasonality in catchment streamflow with summer low flows commonly below 0.01 mm/h and peak flows that can reach 6 mm/h during winter storms of moderate intensity.

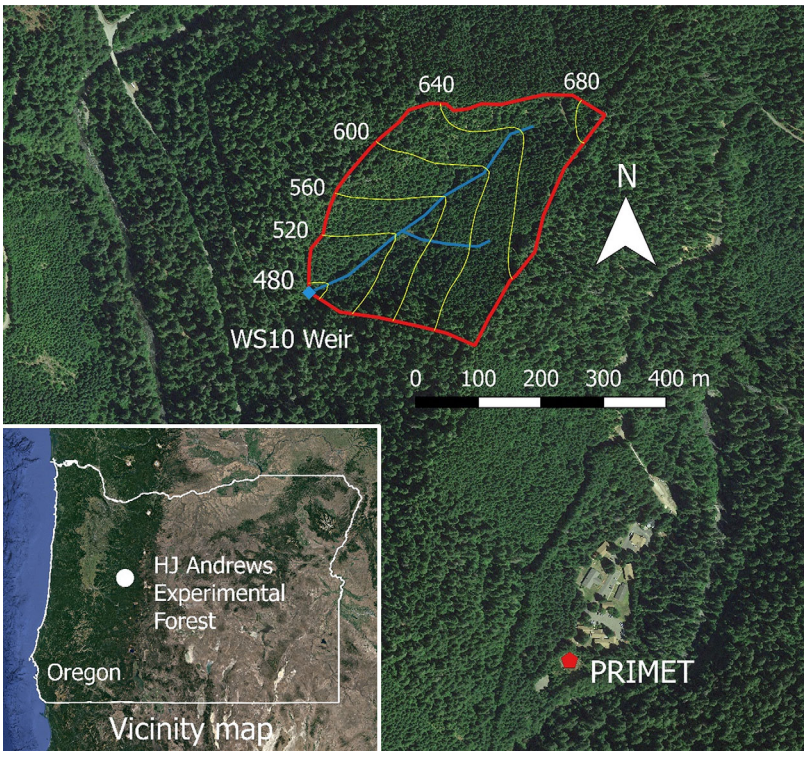

Figure 1. Map of WS10 in the HJA, showing the location of the PRIMET meteorological station nearby, and the location of HJA in Oregon, USA. The outlet weir is located at coordinates 44.2169°N and 122.2611°W. Yellow lines indicate the elevation in meters above sea level. Background map data: Google.

WS10 mostly consists of short (<200 m) and steep (30–45°) hillslopes, with elevations ranging from 473 to 680 m.a.s.l. The catchment is covered by Douglas-fir trees (*Pseudotsuga menziesii*), which regenerated naturally following a clearcut in 1975. Soil depth varies from 1.5 to 4.2 m, with an average of 3 m (Sayama & McDonnell, 2009). Soils are identified as gravelly clay loams at the surface, as gravelly silty clay loams or clay loams in lower layers, and as gravelly clays or clay loams in the subsoils (Harr, 1977). Soil total porosity is 60% on average, and varies little with depth. The soils in WS10 are highly conductive (saturated hydraulic conductivities well above 300 cm/h at the surface) due to their aggregated structure and their high drainable porosity, which in average declines with depth from 23% at the surface to 5% at 1.5 m depth (Dyrness, 1969; Harr, 1977). No overland flow has been observed in WS10 (McGuire et al., 2005). Moreover, preferential flow strongly influences runoff generation, as revealed by the rapid transport of tracers applied on one of the WS10 hillslopes (McGuire et al., 2007; McGuire & McDonnell, 2010). WS10 is underlain by volcanic bedrock including andesitic and dacitic tuff and coarse breccia (Swanson & James, 1975), which is considered mostly impermeable except in weathered and highly fractured areas that can rapidly transfer groundwater reaching the regolith-bedrock interface laterally (Gabrielli et al., 2012; van Verseveld et al., 2017). Poorly permeable, 1–7 m thick partially weathered saprolite underlies the soils (Harr & McCorison, 1979). Unweathered bedrock is found at 0.4–0.6 m depth on the stream-hillslope interface and at 3–8 m depth at the catchment divide. Debris flows occur periodically in WS10 (e.g., 1986, 1996), and maintain a narrow and steep stream channel with apparent bedrock on 60% of its length upstream from the outlet.

McGuire and McDonnell (2010) summarized the current understanding of water flow paths and streamflow travel times in WS10 in a perceptual model. Different streamflow generation mechanisms are activated sequentially depending on the wetness state: dry state in summer (June to October), transition states in fall (October to December) and in spring (April to June), and wet state in winter (December to April). During dry periods, groundwater above the soil-bedrock interface provides base flow with an age of 1–2 years. During wet-up periods in fall, water from rainfall events moves vertically in the soils as unsaturated flow, recharging gradually the deeper soils in the hillslopes, as suggested by stable isotope patterns at different soil depths (Brooks et al., 2010). Water from rainfall events can also reach the stream in less than 2 days by preferential flow. Vertical preferential flow occurs in the hillslope soils while lateral preferential flow occurs in the fractured bedrock at the soil-bedrock interface, as derived from tracer experiments (McGuire et al., 2007; van Verseveld et al., 2017), and hydrogeological observations (Gabrielli et al., 2012). After the wet-up period, soil saturation expands upslope (Harr, 1977) and mobilizes the soil water recharged over the last month, creating lateral saturated flow. This may cause a seasonality of streamflow travel times in WS10 with the onset of connectivity between the hillslopes and the stream. McGuire and McDonnell (2010) showed that the connection and disconnection of hillslopes from the stream creates hysteresis in the hillslope-catchment discharge relationship. Hillslopes provide water that is contrastingly younger than the groundwater from the bedrock (Gabrielli et al., 2012).

2.2. Data Set

Precipitation and air temperature were recorded at the PRIMET meteorological station located less than 1 km away from the WS10 gauge, at a similar elevation (436 m.a.s.l.). Potential evapotranspiration (PET) was calculated with Thornthwaite's method (Thornthwaite, 1948), based on PRIMET air temperature measured 150 cm above ground. Streamflow data were converted with a rating curve from water levels measured at 15 min intervals (Rothacher, 2016). We used a 2 year time series of ^{18}O in precipitation and catchment streamflow spanning from January 2001 to February 2003 and described by McGuire et al. (2005) (Figure 2). Precipitation was sampled as weekly bulk samples at the PRIMET station. Additionally, sequential rainfall samples (4.4 mm increments, i.e., on average, one sample every 20 h) were collected in WS10 during fall and winter 2002 (McGuire & McDonnell, 2010). We interpolated an hourly ^{18}O signature in precipitation by assuming that the precipitation $\delta^{18}O$ value between two consecutive samples had the value of the last sample. Streamflow was manually sampled at weekly intervals, including periods (a few days to a week) of subhourly to subdaily automatic sampling. When several stream samples were taken in less than 1 h, a flow-weighted value was calculated for the hourly interval. The ^{18}O analysis procedure is described in McGuire et al. (2005).

2.3. Catchment Model

A conceptual catchment model was employed to simulate water storage and water fluxes in WS10 (Figure 3), as well as the transport of ^{18}O (or any other tracer) (Table 2). A total of nine parameters were needed (Table 1)

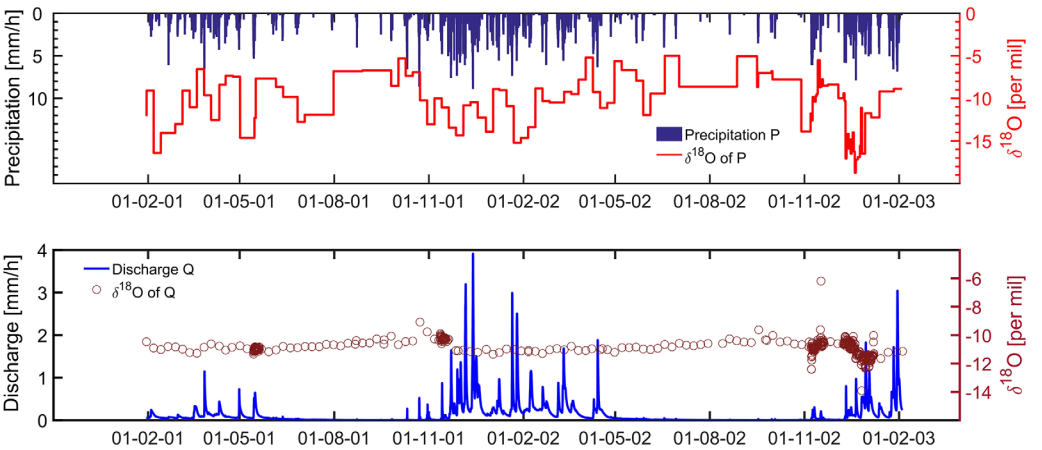

Figure 2. (top) Precipitation rates and precipitation δ^{18}O values used for this study. (bottom) Discharge in WS10 outlet and streamflow δ^{18}O values used for this study.

and determined from calibration to observed data (see section 2.5 for details on calibration). We want to stress that the main purpose of the model was to provide physically meaningful estimates of the water storage in different compartments (i.e., soil water and groundwater) and of the fluxes from and between them. The model results were used to derive time-varying RTDs, and streamflow TTDs and SAS functions (see section for 2.6 details on how these were determined). We used the successful model realizations as the best approximation of the catchment and its internal flow paths. This approach was previously described and used for example by Benettin et al. (2015b), who successfully applied a similar model structure to the Upper Hafren catchment in Plynlimon, Wales. In this study, we justified the validity of the approach and of the reliability of its estimates of water storage and fluxes by comparing the model-simulated streamflow and δ^{18}O in streamflow to the observed data in WS10.

The model structure was chosen because it is consistent with the experimental observations of the water flow paths in WS10 summarized by McGuire and McDonnell (2010). These flow paths consist of groundwater flow in the bedrock, and saturated and unsaturated flow in the hillslope soils during the wet season. The model uses two reservoirs connected in a series (one after the other) and in parallel (the first reservoir can bypass the second) (Figure 3). The upper reservoir represents the storage of water in the soils and subsoils

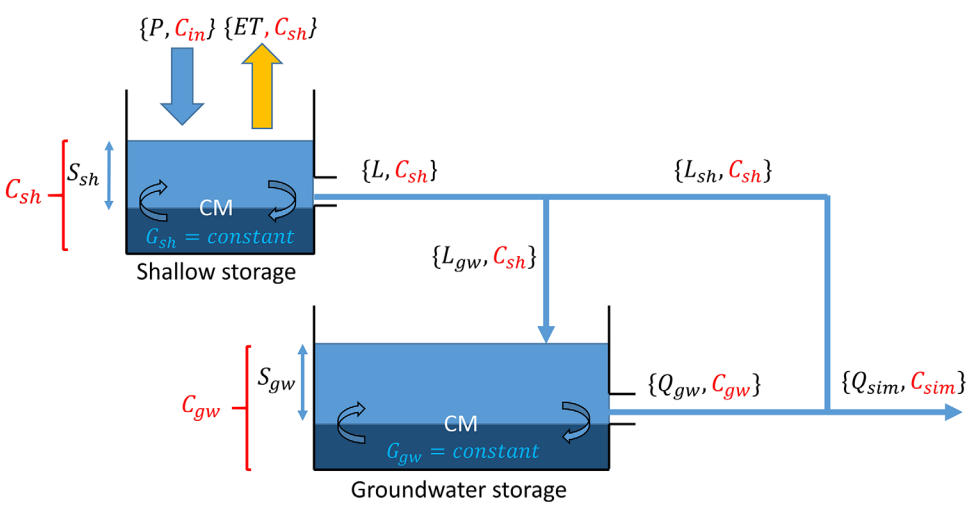

Figure 3. Conceptual catchment model employed for WS10 in this study. The inflows and outflows of each reservoir are indicated in pairs {flux, concentration}, representing the water fluxes and their associated tracer concentration in red font (i.e., δ^{18}O values). The passive storage volumes are pictured in dark blue. CM stands for Complete Mixing (see section 2.3.).

Table 1
Model Parameters

Name	Symbol	Unit	Description
ET magnifier	Ψ	(−)	Coefficient increasing the magnitude of ET
Reference partition coefficient	λ_0	(−)	Maximum fraction of streamflow made of direct contributions from the shallow storage reservoir
Discharge coefficient	μ_Q	mm/h	Magnitude coefficient in the storage-discharge relationships
Shallow storage exponent	β_{sh}	(−)	Shape coefficient of the shallow reservoir storage-discharge relationship
Groundwater storage exponent	β_{gw}	(−)	Shape coefficient of the groundwater reservoir storage-discharge relationship
Shallow storage capacity	D_{sh}	mm	Capacity of the shallow storage reservoir
Groundwater storage capacity[a]	D_{gw}	mm	Capacity of the groundwater storage reservoir
Shallow passive storage	G_{sh}	mm	Amount of water contributing only to mixing with the shallow storage reservoir
Groundwater passive storage	G_{gw}	mm	Amount of water contributing only to mixing with the groundwater storage reservoir

[a]This parameter was treated differently in the calibration. See section 2.5 for details.

in the hillslopes (called "shallow storage"), which is able to generate a rapid response to precipitation during wetter periods. The lower reservoir represents the storage of water in the weathered and unweathered bedrock (called "groundwater storage"), which provides base flow and remains active during the prolonged dry periods in summer.

We distinguished two forms of water storage in each reservoir. Active storage can freely drain by gravity and is directly available to generate discharge. In the shallow storage reservoir, active storage is the state variable S_{sh}, while this variable is called S_{gw} in the groundwater storage reservoir (Figure 3). Passive storage (parameters G_{sh} and G_{gw}, Table 1 and Figure 3) does not modify the hydrological response of the reservoir but causes a dampening of the tracer response by mixing. It is essentially as if the passive storage was exchanging water molecules with the active storage (and incoming precipitation) at an infinite rate. We assumed constant passive storage, as is common in hydrological transport studies employing conceptual models (Benettin et al., 2015a; Fenicia et al., 2010; Hrachowitz et al., 2013). Thus, the hydrological storage-discharge equations only involve the active storage, while ^{18}O tracer transport equations use both the active and the passive storage (see Table 2 for equation details).

In this study, we used the Complete Mixing (CM) assumption that considers that each modeled reservoir acts as a fully-mixed system. This means that for each reservoir, all outflows have a $\delta^{18}O$ concentration equal to the mean reservoir $\delta^{18}O$, which involves the total reservoir storage (active + passive). The CM assumption implies that the distributions of water ages in the reservoir and each of its outflows are the same, which is known as Random Sampling (RS) (see section 2.6). The simulated tracer response of the catchment was governed by the relative contributions of the shallow and the groundwater storage to streamflow. Although each reservoir is a fully mixed system, the overall system is not fully mixed, which is consistent with previous findings for WS10 (Klaus et al., 2015). This is because each reservoir generally has a different $\delta^{18}O$, a different RTD, and contributes in varying degrees to streamflow (Benettin et al., 2015b).

Table 2
Hydrological and Transport Equations Used in the Model

State variable	Units	Balance equation[a]	Constitutive functions[b]
S_{sh}	mm	$\frac{dS_{sh}}{dt}(t)=P(t)-ET(t)-L(t)$	$L(t)=\mu_Q\ s(t)^{\beta_{sh}}$ $L_{sh}(t)=\lambda_0\ s(t)\ L(t)$
S_{gw}	mm	$\frac{dS_{gw}}{dt}(t)=L_{gw}(t)-Q_{gw}(t)$	$L_{gw}(t)=(1-\lambda_0\ s(t))\ L(t)$ $Q_{gw}(t)=\mu_Q\left(\frac{S_{gw}(t)}{D_{gw}}\right)^{\beta_{gw}}$
M_{sh}	mm ‰	$\frac{dM_{sh}}{dt}=P(t)\ C_{in}(t)-(ET(t)+L(t))\ C_{sh}(t))$	$C_{sh}(t)=\frac{M_{sh}(t)}{S_{sh}(t)+G_{sh}}$
M_{gw}	mm ‰	$\frac{dM_{gw}}{dt}=L_{gw}(t)\ C_{sh}(t)-Q_{gw}(t)\ C_{gw}(t)$	$C_{gw}(t)=\frac{M_{gw}(t)}{S_{gw}(t)+G_{gw}}$

[a]See Figure 3 for a visual interpretation of the balance equations. See section 2.4 for details on the equations and on the terms used in the equations. [b]$s(t)=S_{sh}(t)/(n\times D_{sh})$, see section 2.4.

2.4. Hydrological and Transport Equations

Simulations of water and tracer mass used four state variables. The first two state variables were shallow reservoir active storage S_{sh} and shallow reservoir $\delta^{18}O$ mass M_{sh}. The latter was taken as the product of total shallow storage ($S_{sh} + G_{sh}$) and $\delta^{18}O$ concentration in the shallow storage C_{sh}. The last two state variables were groundwater reservoir active storage S_{gw} and groundwater reservoir $\delta^{18}O$ mass M_{gw}. The latter was taken as the product of the total groundwater storage ($S_{gw} + G_{gw}$) and $\delta^{18}O$ concentration in the groundwater storage C_{gw}. These four state variables changed according to their balance equation involving model forcings: measured precipitation rates P and calculated evapotranspiration rates ET; and constitutive flux functions with their parameters (Tables 1 and 2). Some constitutive functions used the variable s(t) that we defined as the active shallow storage normalized by the maximum value it can take, as in Benettin et al. (2015b) (equation (1)):

$$s(t) = \frac{S_{sh}(t)}{n \times D_{sh}} \tag{1}$$

where D_{sh} is shallow storage capacity (mm), a calibrated parameter, and n is the model soil drainable porosity, a fixed parameter. This is consistent with our description of the model reservoirs, where active storage is at most the volume of water that can freely drain by gravity. We used a constant n value equal to the upper limit of drainable porosity in WS10, which is n = 23% in the upper soil (Harr, 1977). Actual ET was calculated from PET in equation (2):

$$ET(t) = \Psi \ \frac{s(t)(1+m)}{s(t)+m} \ PET(t) \tag{2}$$

where ψ is a calibrated parameter that enhances the seasonal amplitudes of ET and allows a good agreement between ET and the long-term average difference P-Q (1980–2003). m = 0.5 is a fixed smoothing parameter used to ensure numerical stability of the solution by quickly reducing ET as water availability in soils (represented by s(t)) decreases (cf. Fenicia et al., 2016). Discharge from each reservoir was formulated as a power function of the reservoir storage normalized by the maximum value it can take (Table 2): $Q(t) = \mu_Q \left(\frac{S(t)}{max\,(S)}\right)^{\beta}$ where β is a dimensionless shape coefficient. For the shallow storage, the normalized storage s(t) (equation (1)) was used, whereas for the groundwater storage we divided the active storage S_{gw} by the calibrated parameter D_{gw} representing the groundwater active storage capacity in mm of water (Table 1). The magnitude coefficient μ_Q is an upper bound of the discharge from the reservoirs, with the same units as the observed streamflow (mm/h). μ_Q acts as a scaling factor for the storage-discharge relationships, depending on the average value of the ratio $\left(\frac{S(t)}{max\,(S)}\right)^{\beta}$. We used μ_Q for the shallow and the groundwater storages to limit the number of parameters (c.f. Benettin et al., 2015b). The normalization of the storage-discharge relationship by the maximum storage has a number of advantages compared to the classical nonlinear storage-discharge formulation. It leads to more intuitive parameter units (mm and mm/h only), reduces the trade-off effects between shape and magnitude coefficients in the calibration, and it helps estimating a priori around what values the storages will fluctuate (Kirchner, 2016). Discharge from the shallow storage contributes directly to streamflow (L_{sh}) and recharges the groundwater reservoir (L_{gw}) depending on s(t). At the catchment outlet, the simulated discharge was calculated as (equation (3)):

$$Q_{sim}(t) = L_{sh}(t) + Q_{gw}(t) \tag{3}$$

and the simulated streamflow $\delta^{18}O$ value was calculated as (equation (4)):

$$C_{sim}(t) = \frac{L_{sh}(t) \ C_{sh}(t) + Q_{gw}(t) \ C_{gw}(t)}{Q_{sim}(t)} \tag{4}$$

2.5. Numerical Schemes and Calibration Procedure

Each mass balance equation (Table 2) was solved numerically using two different schemes and different time steps depending on the period of interest (P_1 or P_2).

P_1 is a warm-up period of 21 years (1980–2001). Storage values were initialized at the start of P_1 as 50% of the maximum capacity of the shallow storage and 80% of the maximum capacity of the groundwater storage. Both reservoirs were assigned the average streamflow ^{18}O signature (over 2001–2003) $\delta^{18}O = -10.9‰$.

Table 3
Prior Distributions of the Calibrated Parameters

Parameter	Unit	Prior distribution[a]
Ψ	(−)	wbl(1.6, 5)
λ_0	(−)	unif(0, 1)
μ_Q	mm/h	logn(2.43, 0.8)
β_{sh}	(−)	unif(0, 100)
β_{gw}	(−)	logn(4.62, 0.7)
D_{sh}	mm	unif(0, 3000)
D_{gw}	mm	[b]
G_{sh}	mm	unif(0, 3000)
G_{gw}	mm	unif(0, 5000)

[a]wbl(a, b): Weibull distribution with scale parameter a and shape parameter b. unif(min, max): Uniform distribution between min and max. logn(μ, σ): lognormal distribution with parameters μ and σ. [b]This parameter was treated differently, see section 2.5.

We used the precipitation amounts and PET measured at PRIMET and looped back the 2 year record of $\delta^{18}O$ data from 1980 to 2001 to run the model for 21 years. The aim of this warm-up was to remove the impact of the initialization of storage values, the impact of the initial tracer masses, and the influence of the initial residence time distributions on the simulations during period P_2. To reduce the computation time and the memory requirements of the warm-up period, we used daily time steps and an Implicit Euler scheme to solve the mass balance equations without divergence from the solution.

P_2 is the period from January 2001 to February 2003, which we used to calibrate model parameters and interpret the water age results. We employed an Explicit Euler scheme to solve mass balance equations efficiently at hourly time steps. The hourly time steps were sufficiently small so that the solution converged. The hourly time steps also increased the precision of the numerical solution compared to the warm-up period (which has daily time steps), since the numerical errors are in these two numerical schemes directly proportional to the time step size.

The hydrological and transport parameters (Table 1) were calibrated using a single objective (but multicriteria) Monte Carlo approach, which consists of the following sequence of operations, repeated in a loop:

1. Sample all calibration parameters simultaneously from their prior distributions (Table 3).
2. Run the model with the selected parameter set over periods P_1 and P_2.
3. Evaluate model performance over period P_2 with the selected parameter set, by comparing the simulations with the observations. This is done for multiple performance criteria simultaneously, and these are summed into a single objective function.

We repeated this procedure 200,000 times to sample parameter sets. Initial calibration tests showed a correlation between the β_{gw} and D_{gw} parameters. To remove the existing trade-off effects between the groundwater storage exponent β_{gw} and groundwater storage capacity D_{gw}, a storage-discharge relationship was deduced from multiple recession segments with a Master Recession Curve (MRC) analysis, using the matching-strip algorithm of Lamb and Beven (1997). The groundwater reservoir storage-discharge relationship could then be expressed in the model parameter space as the functional relationship $D_{gw} = 30\ \beta_{gw}$. This method was described in detail and successfully used in various catchments in the Alzette River basin in Luxembourg (Fenicia et al., 2006). Thus, D_{gw} was not treated like the other eight free calibration parameters, but was deduced from the values of β_{gw} every time a new parameter set was selected.

Parameter prior distributions (Table 3) were used in order to make sure that the Monte Carlo simulation sampled certain parameters more often in certain ranges of interest. The Weibull distribution was used for parameter ψ to allow a negative skew (i.e., emphasis on lower values). The Lognormal distribution was chosen for parameters μ_Q and β_{gw} to allow a positive skew (i.e., emphasis on higher values). The parameters of the distributions were chosen so that the mode of the distributions was located at values that we judged more appropriate for WS10 and so that the variance around the mode was not too restrictive for the Monte Carlo approach. Choosing a = 1.6 (value of the mode) and b = 5 (measure of the spread) in the Weibull distribution of the parameter ψ (Table 3) constrained ψ to values allowing a good agreement between simulated ET and the observed average difference P-Q (1980–2003). Using ψ was necessary to close the water balance, because average PET estimates were found to be 120 mm/yr below the average difference P-Q (over 1980–2003) (see also Waichler et al., 2005). This choice of the prior for ψ also prevented ET rates from exceeding 5 mm/d, which is the upper limit for WS10 (Barnard et al., 2010). Choosing $\mu = 2.43$ and $\sigma = 0.8$ in the Lognormal distribution of the parameter μ_Q allowed a good agreement between observed and simulated maximum streamflow (around 6 mm/h for the period 1980–2003), by placing the mode of the distribution at $e^{\mu-\sigma^2} \approx 6$ and guaranteeing a sufficient positive skew. Finally, for the parameter β_{gw}, choosing $\mu = 4.62$ and $\sigma = 0.7$ in the Lognormal distribution placed the mode at $e^{\mu-\sigma^2} \approx 62$. This yielded groundwater storage values consistent with the catchment storage in WS10 estimated from its time invariant streamflow Mean Travel Time (MTT) of 1.2 years (McGuire et al., 2005), since we used the relationship $D_{gw} = 30\ \beta_{gw}$ and assumed that $MTT = D_{gw}/Q_{avg}$, where Q_{avg} is observed average annual streamflow (1980–2003).

Model performance Φ was evaluated for the 200,000 parameter sets over period P_2 simultaneously for the hourly streamflow data (observed Q and simulated Q_{sim}) and for the observed $\delta^{18}O$ and simulated $\delta^{18}O$ (C_{sim}) at the catchment outlet with (equation (5)):

$$\Phi = NSE_Q + NSE_{logQ} + V_Q + NSE_{\delta^{18}O} + V_{\delta^{18}O} \tag{5}$$

where NSE stands for Nash-Sutcliffe Efficiency (Nash & Sutcliffe, 1970) and V stands for Volumetric Efficiency (Criss & Winston, 2008). We chose those performance metrics to emphasize various parts of the simulated flows Q and $\delta^{18}O$ (correspondence in peaks reflected in NSE, recessions reflected in NSE_{log}, and long-term trends reflected in V). This means that all our results and conclusions drawn from the use of the model are conditional on the simultaneous fit of the model to discharge and $\delta^{18}O$.

The 200,000 parameter sets were ranked by decreasing Φ. We kept the top-ranked 1,000 parameter sets as behavioral (i.e., the best 0.5% parameters) and discarded the others. Parameter histograms were generated from the behavioral parameter sets. For travel time calculations, we selected the calibrated parameter set consisting of the most common occurring value for each parameter from the histograms (cf. Benettin et al, 2015b). We also run a posteriori simulation with this identified parameter set to confirm that the associated model performance Φ was among the 1,000 best, as this specific combination was not sampled within the 200,000 parameter sets.

2.6. Residence Time Distributions, Streamflow Travel Time Distributions and StorAge Selection Functions

We calculated RTDs, and streamflow TTDs and SAS functions by tracking water ages in the calibrated catchment model. The approach consists of solving the Master Equation (ME) (equation (6)) numerically for each model reservoir R, yielding its residence time distribution, p_R, at every moment (Botter et al., 2011):

$$\frac{\partial}{\partial t}(S_R(t)\ p_R(T,t)) = -S_R(t)\ \frac{\partial p_R(T,t)}{\partial T} - \sum_{k=1}^{n} Q_k(t)\ p_k(T,t) \tag{6}$$

where T is water age since it entered the catchment surface as precipitation, S_R is the total storage of the reservoir (active + passive), and p_k is the travel time distribution of the outflow Q_k from the reservoir R (in this case discharge and/or ET fluxes). Water storage in each reservoir and fluxes between reservoirs were necessary to solve the equation (equation (6)). These quantities were provided by the simulation results from the calibrated conceptual model.

The RS scheme implies that outflows from a given reservoir draw water ages proportionally to their relative presence in storage, which corresponds to SAS functions ω_k equal to 1 across all ages T and all times t for each outflow Q_k. This means that the probability that a water parcel has the age T in outflow k at time t is the probability that a water parcel in the corresponding storage has the age T at time t (equation (7)):

$$p_k(T,t) = \omega_k(T,t)\ p_R(T,t) = 1 \times p_R(T,t) \tag{7}$$

Boundary conditions for the ME were defined by precipitation inputs with T = 0 in storage at every time t (equation (8)):

$$p_R(0,t) = \frac{P(t)}{S_R(t)} \tag{8}$$

Initial conditions for the ME were specified as an exponential distribution of water ages in storage at t = 0 (equation (9)), with a mean T_0 = 1.2 years (McGuire et al., 2005):

$$p_R(T,0) = \frac{1}{T_0}\exp\left(-\frac{T}{T_0}\right) \tag{9}$$

The effect of these initial RTDs in storage was removed by the 21 year warm-up period P_1 (1980–2001). This method was shown to have little impact on travel time estimates in the following period P_2 used for the interpretations of the results (cf. Hrachowitz et al., 2011).

The overall streamflow TTD, p_Q was calculated as a flow-weighted TTD of the different contributions of the reservoirs to streamflow (equation (10)):

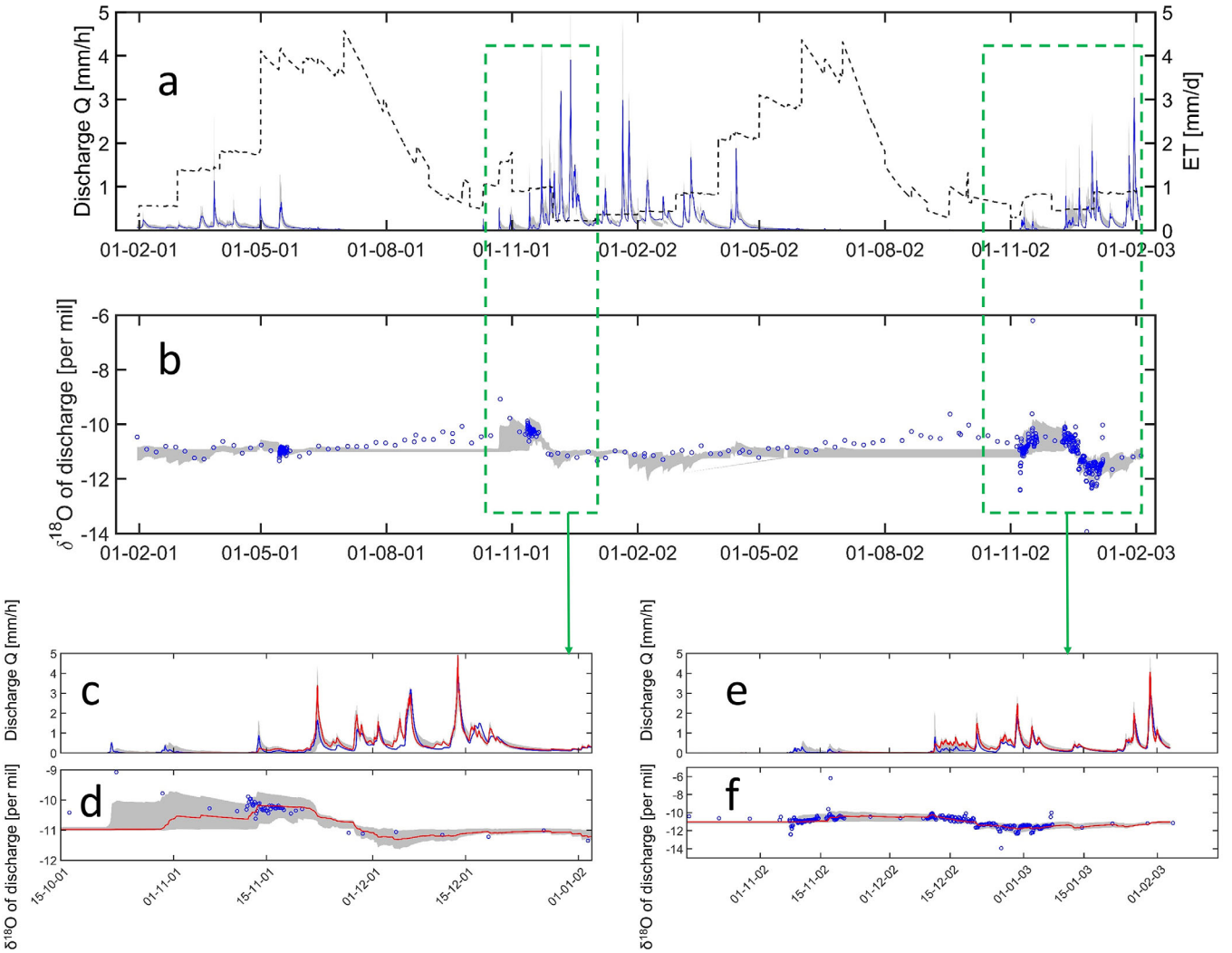

Figure 4. (a, c, and e) Simulation envelopes of the behavioral solutions (gray bands), for streamflow and (b, d, and f) its $\delta^{18}O$ values, (a and b) for the whole simulation period, including simulated ET (dashed blacked line), and for wet-up periods of (c and d) 2001 and (e and f) 2002, including the calibrated model simulation (red line). Observations are in blue.

$$p_Q(T,t) = \frac{L_{sh}(t)\ p_{sh}(T,t) + Q_{gw}(t)\ p_{gw}(T,t)}{Q_{sim}(t)} \tag{10}$$

The overall catchment RTD, p_S was calculated as a storage-weighted RTD including all forms of storage (equation (11)):

$$p_S(T,t) = \frac{(S_{sh}(t)+G_{sh})\,p_{sh}(T,t) + (S_{gw}(t)+G_{gw})\ p_{gw}(T,t)}{S_{sh}(t)+S_{gw}(t)+G_{sh}+G_{gw}} \tag{11}$$

The overall streamflow SAS function ω_Q was calculated as the ratio of the overall streamflow TTD and the overall RTD (equation (12)):

$$\omega_Q(T,t) = \frac{p_Q(T,t)}{p_S(T,t)} \tag{12}$$

Note that ω_Q represents the contributions of both reservoirs to streamflow, and is different from the individual SAS functions for each reservoir ω_k, which are all equal to 1. The dynamics of the streamflow SAS function ω_Q were therefore mostly governed by the relative contributions of the shallow and the groundwater reservoirs with their respective RTDs.

Table 4
Model Performance Metrics

Variable	NSE[a]	VE[b]
Q	**0.85** (0.74–0.89)	**0.67** (0.57–0.7)
log(Q)	**0.73** (0.60–0.77)	
$\delta^{18}O$	**0.51** (0.31–0.57)	**1.02** (0.99–1.03)

Note. Bold values: calibrated model; ranges of the behavioral solutions in parentheses.
[a]Nash-Sutcliffe Efficiency (Nash & Sutcliffe, 1970). [b]Volumetric Efficiency (Criss & Winston, 2008).

3. Results

3.1. Simulated Q, ET, $\delta^{18}O$, and Parameter Distributions

The calibrated model successfully reproduced streamflow seasonality, alternating between the high and the low flows (Figure 4) with NSE = 0.85 over the period P_2 (Table 4). The modeled ET in WS10 averaged 576 mm/yr (2001–2003), consistent with past ET estimates using a monthly Thornthwaite method with the same climate station (Rothacheret al., 1967). ET varied strongly across seasons. During the summer, ET peaked at around 5 mm/d, which is consistent with estimates using the Penman-Monteith method (Monteith, 1965) over a summer period in WS10 (Barnard et al., 2010). In summer, ET depleted the water available in the soils for generating streamflow. In winter, modeled ET decreased to about 1 mm/d, consistent with estimates by McGuire et al. (2007). Streamflow $\delta^{18}O$ was well reproduced by the model (Figure 4) with NSE = 0.51 (Table 4). However, the calibrated model partly failed to reproduce the first $\delta^{18}O$ peaks in the wet-ups of October 2001 and 2002. Furthermore, simulated and observed $\delta^{18}O$ deviated through low flows in the summer (when streamflow was near-zero and little rainfall-runoff response occurred). Generally, behavioral parameter ranges were rather wide (spanning 1–2 orders of magnitude, Figure 5 and Table 5), except for the parameters ψ, λ_0, μ_Q, and β_{sh}. The behavioral distributions for parameters ψ, μ_Q, and β_{gw} were rather similar to the prior distributions, which indicates that the prior distributions were decisive in the calibration. This introduced a certain degree of subjectivity.

3.2. Dependence of the Streamflow SAS Functions on Catchment Storage

We used the dynamic storage metric S_d as a proxy of catchment wetness (equation (13)):

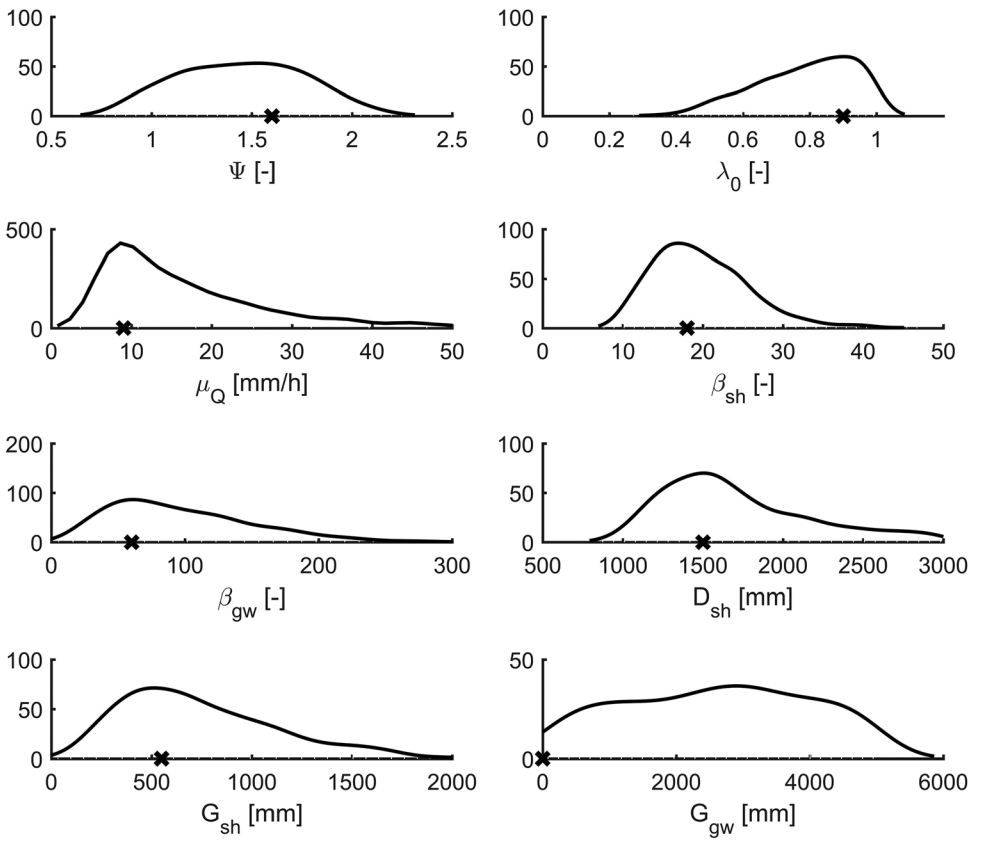

Figure 5. Histograms of the 1,000 best parameter sets (smoothed by a normal kernel distribution), and calibrated parameter values (crosses). Units in *y* axis are nondimensional numbers per parameter value.

Table 5
Calibrated Parameter Values and Parameter Ranges of the Behavioral Solutions

Parameter	Unit	Calibrated value	Behavioral range[a]
Ψ	(−)	1.6	0.88–2.1
λ_0	(−)	0.9	0.47–0.99
μ_Q	mm/h	9	5.8–60
β_{sh}	(−)	18	11–34
β_{gw}	(−)	60	22–2.2×10^2
D_{sh}	mm	1,500	1.1×10^3 to 2.9×10^3
D_{gw}	mm	1,800[b]	6.6×10^2 to 6.6×10^3
G_{sh}	mm	550	1.9×10^2 to 1.6×10^3
G_{gw}	mm	0[c]	1.6×10^2 to 4.9×10^3

[a]2.5–97.5 percentile range of the distributions in Figure 5. [b]This parameter was treated differently, see section 2.5. [c]Parameter constrained to 0, see section 4.1.

$$S_d(t) = S_{sh}(t) + S_{gw}(t) - \min\left(S_{sh} + S_{gw}\right) \quad (13)$$

This metric ranged from 0 mm, when the active storage ($S_{sh} + S_{gw}$) was at its minimum (around September), to almost 400 mm, when the active storage reached its maximum (around January). Distinct patterns of streamflow SAS functions could be identified, depending on the value of S_d (Figure 6). During dry periods, when S_d approached 0 (red curves), streamflow preferentially selected older water. Younger water was preferentially selected during wet periods (blue curves), when S_d approached its maximum (about 400 mm). This is consistent with the definition of the ISE. However, during transition periods, when S_d took intermediate values (e.g., 175–275 mm), streamflow SAS functions did not vary regularly with S_d, as they alternated rapidly between a preference for younger and a preference for older water (Figure 6). This indicates that during transition periods, the ISE was not always valid. The streamflow SAS functions in WS10 also displayed noticeable plateaus. For example, the top purple curves (Figure 6) are flat between $P_S = 0$ and $P_S = 0.2$, which shows that the youngest 20% of the water particles stored in the catchment were equally mobilized to generate discharge at that time. Such plateaus can be followed by sharp vertical variations as seen for P_S slightly above 0.2 (Figure 6, purple curves). This shows that the oldest 80% of the water particles were significantly less mobilized to generate discharge compared to the youngest 20% at that time, suggesting a strong variability of flow paths.

3.3. Inverse Storage Effect (ISE) in WS10

Let t_m be the time when the catchment storage S reaches its minimum S_{min} and t_M the time when the catchment storage reaches its maximum S_{MAX}. The sign of the following metric χ generally defines the increase or decrease in the preference of streamflow for younger water, for increasing storage values (equation (14)):

$$\chi = \frac{\omega_Q(P_S=0,\ t_M) - \omega_Q(P_S=0,\ t_m)}{S_{MAX} - S_{min}} \quad (14)$$

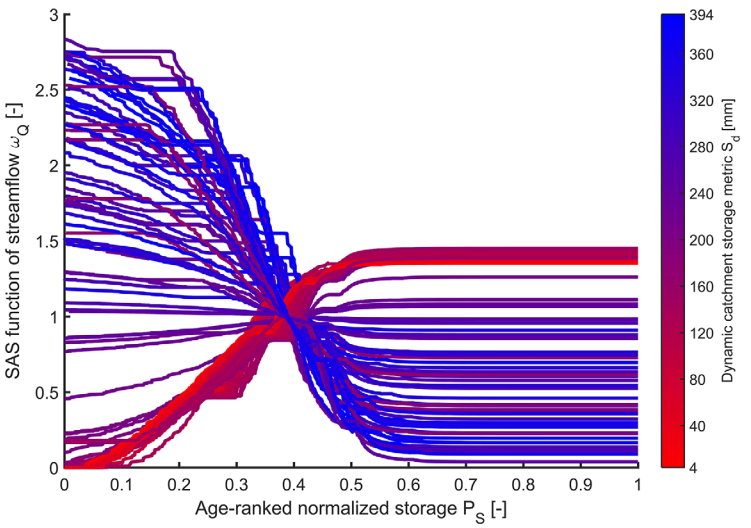

Figure 6. Streamflow SAS functions $\omega_Q(T,t)$ for different dynamic storage values $S_d(t)$. Each curve represents a different time t, associated with a color from red to blue, depending on the value $S_d(t)$. We used a change of variables $T \rightarrow P_S(T,t)$ for the SAS functions ω_Q ($P_S(T,t)$, t), where P_S is the cumulative residence time distribution (i.e., age-ranked normalized storage). Younger ages in storage are toward the left part of the *x* axis, and a higher amplitude of ω_Q indicates a stronger preference of streamflow for a given age in storage.

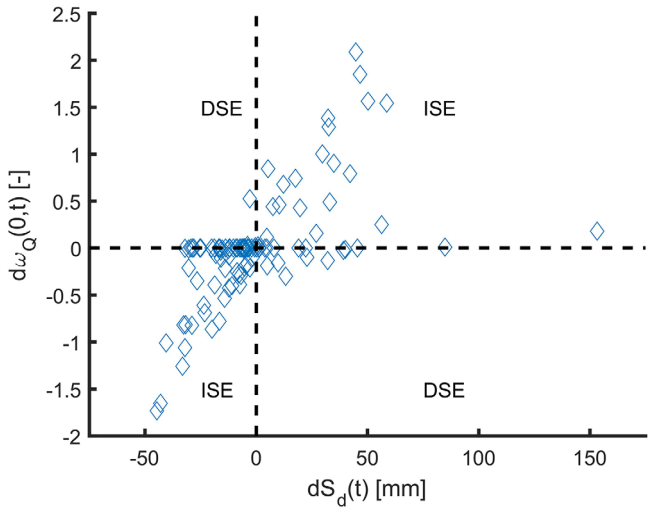

Figure 7. Variations of the streamflow SAS functions ω_Q at age 0 against variations of S_d in time (here we used weekly intervals to compute these variations). When dS_d and $d\omega_Q$ have the same sign, the catchment response corresponds to the ISE, otherwise it corresponds to the DSE. For practical calculations, since ω_Q is not defined at all ages for all t, we selected at time t the value of ω_Q at the youngest age T available (in our case up to T = a few days).

Note that in our case, we could compute χ using the dynamic storage metric S_d instead of the absolute storage S, since their time variation was the same. Water age T or age-ranked storage S_T could be used as an alternative variable for ω_Q in equation (14). $\chi > 0$ indicates an ISE overall, while $\chi < 0$ indicates a Direct Storage Effect (DSE) overall. Contrary to the ISE, the DSE is by definition a decrease of young water fractions in discharge for increasing storage (Harman, 2015). In WS10, the ISE is generally the dominating process since $\chi = \frac{2.4}{370\ mm} = 0.065\ mm > 0$.

During transition periods in WS10 (approximately for 175 mm $< S_d <$ 275 mm), the streamflow SAS functions varied strongly while S_d varied little, which prevented the use of a metric similar to χ (e.g., denominator close to 0 when variations of S_d were close to 0). Thus, we needed to compare the variations of ω_Q for the youngest water (i.e., $d\omega_Q(0,t)$) and the variations of S_d (i.e., $dS_d(t)$) in a time-varying way. We compared variations of ω_Q and S_d at weekly intervals, i.e., we compared $\omega_Q(0, t + 1week)$-$\omega_Q(0,t)$ and $S_d(t + 1week)$-$S_d(t)$ (Figure 7). It became apparent that the response of WS10 was mostly in agreement with the ISE (Figure 7). However, there were periods during which $dS_d > 0$ and $d\omega_Q < 0$, i.e., the DSE seemed to apply. A particularly important number of points lay on the $d\omega_Q = 0$ axis for $dS_d < 0$ (Figure 7), which shows that weekly variations in $S_d(t)$ and weekly variations of $\omega_Q(0,t)$ were independent in these moments.

3.4. Streamflow Travel Time Dynamics

The streamflow median travel time (MdTT) in WS10 showed a pronounced seasonality, ranging from less than 100 days during wetter periods to more than 1,300 days during drier periods (Figure 8). Similar to the streamflow SAS functions, the MdTT appeared not to depend only on the value of S_d. When $S_d < 175$ mm, the MdTT was high and it increased as S_d decreased. Conversely, when $S_d > 275$ mm, the MdTT was low and it decreased as S_d increased. Yet, for values of S_d close to these two thresholds, switches between the low and high values of the MdTT occurred. Over the entire range of S_d, MdTT followed a counter-clockwise

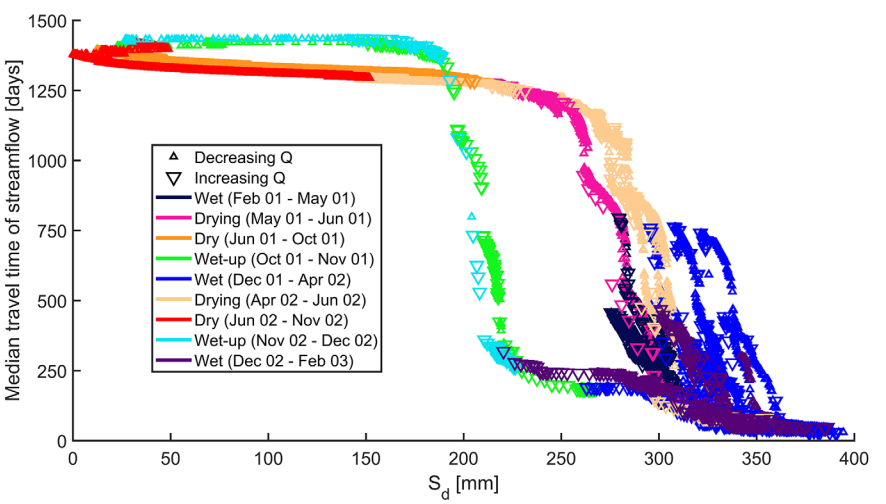

Figure 8. Streamflow Median Travel Time (MdTT) plotted against S_d. The colors of the triangles indicate various hydrological periods that we selected manually: wet-up (when the first fall rainfall-runoff events occur after a long dry period in summer), wet period (when winter larger rainfall events create large runoff events), dry-out (when discharge starts decreasing in spring while ET starts increasing), dry period (when discharge is minimum and PET is maximum in summer). Smaller triangles pointing upward indicate decreases in discharge Q (these are pointing upward because they are generally associated with increases in the MdTT), while bigger triangles pointing downward indicate increases in discharge Q. The main hysteresis loop runs counterclockwise.

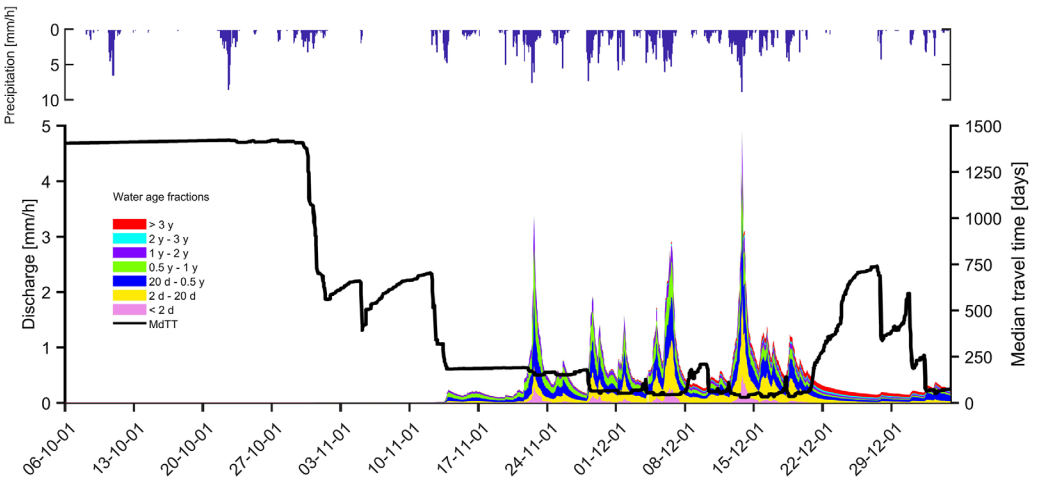

Figure 9. Simulated hydrographs over the beginning of winter 2001, showing the different fractions of streamflow ages in time (age brackets associated with contrasting colors) and the streamflow median travel time MdTT (black curve) in time. The top part of the plot shows precipitation rates. Note that the youngest water fraction is placed at the bottom of the hydrograph to make it more visible.

hysteresis loop. Many MdTT values corresponded to a given S_d, which indicates that the streamflow travel times in streamflow depend on the whole history of storage states. Note that a clockwise hysteresis loop exists for $S_d < 175$ mm only because water is aging steadily. Smaller counterclockwise hysteresis loops are visible for $S_d > 275$ mm and correspond to differences between the rising limb and the falling limb of runoff events (Figure 8).

Water age fractions in streamflow (Figure 9) help understand the observed MdTT patterns. Streamflow volume was dominated by younger water discharged during runoff events. At the beginning of winter 2001, the catchment passed through several states and periods that could be identified as follows (Figure 9):

1. Period 1 (6–27 October 2001), dry catchment state: streamflow is very low, rather constant, and 75% of the water is over 2 years old, which explains the very long MdTT of over 3 years. Water is aging steadily, as indicated by the small and constant increase in the MdTT.
2. Period 2 (27 October to 27 November 2001), wet-up: as soon as the stream starts reacting to precipitation events, even when the streamflow response is so low that it does not show up on the graph (Figure 9), the event water fraction (age < 2 days, pink color) increases rapidly (up to 12%). Young preevent water (2–20 days, yellow color) starts to be mobilized and ranges from 10% to 15% of the total flow. This causes the MdTT to drop significantly to under 2 years. Streamflow increases sharply and consists mostly of water younger than 1 year old.
3. Period 3 (27 November to 20 December 2001), wet state: through the wettest period of winter, the event water fraction slightly decreases (peaking around 10%), whereas young preevent water (2–20 days) becomes more relevant (up to 35% contribution). This causes the MdTT to decrease to less than 6 months. Streamflow is then at its maximum and mostly composed of water younger than 6 months.
4. Period 4 (20 December 2001 to 4 January 2002), recession: event water is not found in streamflow as recession proceeds and rainfall events cease, and young preevent water (2–20 days) contributes to less than 10% of the streamflow. About 50% of streamflow is older than 2 years. Consequently, the MdTT increases to more than 2 years. The system is still in a transitional phase, where event water can still reach the stream rapidly and causes a noticeable drop in the MdTT during precipitation events.

4. Discussion

4.1. Model Parameterization and Performance

The deviation between simulated and observed $\delta^{18}O$ in streamflow during the low-flow period of 2001 and 2002 (Figure 4) suggests an evaporative enrichment of stream water, which was not implemented in the

model. During these periods, discharge was close to zero ($Q \ll 1$ L/s) and the stream was mainly flowing over a bedrock channel without much storage, and likely experienced evaporation. Without additional ^{2}H data, it is unfortunately not possible to plot the stream samples against the Local Meteoric Water Line (LMWL) and confirm the interpretation that water was fractionated by evaporation.

Within this work, we assumed RS for all outflows in the soil and groundwater reservoirs (cf. Benettin et al., 2015b). Yet, Brooks et al. (2010) found that plants may be able to access water in the soils that does not contribute to discharge. The RS assumption we employed here was nevertheless sufficient to satisfactorily simulate ^{18}O tracer dynamics in the WS10 streamflow (NSE > 0.5 for streamflow $\delta^{18}O$), especially after combining the two storages in series-parallel. The related simplicity of representing transport in this way is a major advantage when solving equations numerically. An additional advantage is the parsimonious parameterization, which limits parameter uncertainties. More complex approaches could parameterize the interactions between the active storage and passive storage in the model. Recent studies have used mixing coefficients in conceptual models and concluded that in some cases, the use of partial mixing (PM) could result in better performances in simulating hydrological tracer transport compared to the use of CM (Fenicia et al., 2010; Hrachowitz et al., 2013; McMillan et al., 2012). Yet, in some cases, this improvement came at the cost of more uncertainty due to decreased parameter identifiability (Fenicia et al., 2010; Hrachowitz et al., 2013). Alternatively, the constant SAS functions used in each reservoir in our study could be changed to varying functions of residence times. One could use, for example, time-variant gamma (Harman, 2015), beta (van der Velde et al., 2012, 2015), or power law distributions (Benettin et al., 2017) with respect to reservoir residence times. The parameters of these distributions could be made storage-dependent. The main difficulty in applying such approaches would be finding the minimum additional state variables or parameters required to capture the true hydrological and chemical processes in this catchment (Haraldsson & Sverdrup, 2013) without increasing uncertainties (Fenicia et al., 2010; Page et al., 2007) or attempting to match the data too closely with too complex and unrealistic parameterizations (Kirchner, 2006). Future work may explore the importance of mixing assumptions in WS10, as done at other sites (e.g., van der Velde et al., 2015).

The parameter ranges in this study were similar to other studies using conceptual models calibrated to hydrographs and tracer data (Benettin et al., 2015a, 2015b; Birkel et al., 2011a, 2015; Birkel & Soulsby, 2016; Fenicia et al., 2010; Soulsby et al., 2015b). However, some other catchment transport studies (e.g., Birkel et al., 2010b; Hrachowitz et al., 2013, 2015) found narrower parameter ranges. A meaningful comparison of parameter uncertainty and ranges is yet challenging due to different processes, parameterizations, and calibration methods. Streamflow $\delta^{18}O$ in WS10 is one of the most damped tracer record among a range of well-studied catchments (Tetzlaff et al., 2009) and thus provides less information about transport processes. Most $\delta^{18}O$ samples in WS10 were weekly samples, which may hide more pronounced variations that could be used to identify transport processes (Birkel et al., 2010a; Dunn et al., 2008; Hrachowitz et al., 2011; Kirchner et al., 2004). The damped and low frequency tracer record in WS10 was partly responsible for the parameter uncertainties. These uncertainties were already discussed by McGuire and McDonnell (2006) a decade ago when applying a steady state convolution approach to derive catchment MTT in WS10.

The prior distributions had a noticeable weight in shaping the behavioral parameter distributions (Figure 5). These prior distributions were nevertheless necessary to simulate streamflow values in agreement with discharge measurements (governed by the parameter μ_Q), ET values corresponding to the previous estimates (parameter ψ), and groundwater storage consistent with a previous MTT estimate (parameter β_{gw}) (see section 2.5.). The parameter G_{gw} representing passive groundwater storage was not identifiable (Figure 5), thus we constrained it to 0 mm. The uncertainty of G_{gw} results from the inability of ^{18}O to distinguish the potential contributions of a groundwater volume with residence times over $\sim$2 years, since these contributions barely show variation in $\delta^{18}O$. Constraining old water fractions of the streamflow TTDs requires additional tracers, such as tritium (Stewart et al., 2012). Uncertainty remains in the contributions and the age of old water in WS10. Similar results were found in the Hubbard Brook catchment, NH, USA (using stable isotopes) and in the Upper Hafren catchment, Plynlimon catchment, UK (using chloride) (Benettin et al., 2015a, 2015b). Future work should assess the uncertainties of time-varying travel times and SAS functions to all model parameters using various water age metrics, such as the Median Travel Time (Benettin et al., 2017) in a rigorous uncertainty framework.

4.2. Time-Varying Relationships Between Storage and Water Ages

Our results (Figures 6 and 8) suggest that streamflow SAS functions and travel times in WS10 mostly depend on catchment wetness, which is controlled by the climate seasonality at HJA. Age selection patterns generally followed the ISE (Figure 7) where the fractions of younger water in discharge increase with increasing storage. This study therefore supports the emerging idea that the ISE may be true for most catchments (Benettin et al., 2017; Harman, 2015; Kim et al., 2016; Pangle et al., 2017; Wilusz et al., 2017). The ISE is also consistent with findings from previous streamflow travel time studies in WS10 (Klaus et al., 2015; McGuire et al., 2007; Sayama & McDonnell, 2009) that have not formally studied age selection patterns. However, our study revealed that during transitions from dry to wetter states in fall, and during transitions from wet to drier states in spring, the ISE did not strictly apply in WS10. During these transitions, the changes in the streamflow SAS functions were not linearly related to the changes of catchment storage. In part, we also found a decrease in the fraction of young water for increasing catchment storage. This may point to a DSE-like behavior in a few instances. The marked seasonality of the Mediterranean climate at HJA made it possible to detect this, resulting in rapid and strong storage variations across seasons. However, uncertainty was highest during these transition periods (Figure 4). Hydrological systems are known to be more uncertain during transitions of certain state variables like soil moisture around threshold values (Zehe et al., 2007). Deviations of travel time dynamics from the ISE have been reported at other sites (Klaus et al., 2013; Legout et al., 2007). For example, Klaus et al. (2013) found higher fractions of preevent water (i.e., "old" water) leaving the soil matrix after a certain moisture threshold was exceeded.

Parameterizing SAS functions with respect to catchment storage has recently been demonstrated using one-to-one relationships with age-ranked storage (Harman, 2015; Benettin et al., 2015b, 2017). In WS10, streamflow SAS functions seemed to depend on storage values with a many-to-many relationship (Figures 6 and 7). During transition periods, different storage values could result in a similar age selection pattern. Reciprocally, different age selection patterns could result from the same storage value. In WS10, catchment mixing, i.e., the variability of flow paths integrated at the catchment scale, thus seemed to depend rather on the history of storage states (i.e., hysteretic), and on the spatial distribution of water storage (e.g., in the hillslopes). This is consistent with the observation of hysteresis in hillslope-catchment discharge relationships in a previous study in WS10 (McGuire & McDonnell, 2010). Contributing areas, where water flows through the subsurface down to the stream, can extend far upstream during the rising limb of the hydrograph, and remain in the higher elevations during the falling limb, creating storage-discharge hysteresis (Nippgen et al., 2015). Overall, our findings suggest that storage effects on water age selection (ISE, DSE) may need to be regarded as a time-varying phenomenon in catchments exposed to a marked seasonal climate. In future work, the parameterizations of SAS functions should ideally integrate this behavior.

4.3. Confronting Time-Varying Streamflow Travel Times and SAS Functions to Previous Flow Path Investigations in WS10

The streamflow travel time estimates in this study were similar to the results from previous studies in WS10. We found an average MTT (flow-weighted) of 1.36 years over the simulated period (2001–2003). Previous studies reported a MTT of 1.2 ± 0.29 years (McGuire et al., 2005), 0.47 years (Sayama & McDonnell, 2009), and 1.1 years (Klaus et al., 2015), even though different approaches were used. The relatively low MTT of Sayama and McDonnell (2009) may be attributed to the fact that their model did not rely on tracer data but only hydrographs to constrain the predictions. The ^{18}O time series contains more information about the velocity of water particles than streamflow data alone, which is more informative about the celerity of subsurface water pressure waves. Incorporating tracer data into the models is known to affect the estimation of parameters and thus water velocities and travel times (McDonnell & Beven, 2014; McGuire et al., 2007; Scaini et al., 2017; van Verseveld et al., 2017; Vaché & McDonnell, 2006). This clearly shows that estimated travel times that are not benchmarked against tracer data must be taken with caution (cf. Danesh-Yazdi et al., 2018). Nevertheless, the streamflow travel time dynamics followed climate seasonality (Figure 9), showing a clear climate control on the MTT in WS10, consistent with previous studies (Klaus et al., 2015; Sayama & McDonnell, 2009) This is consistent with findings from other sites (Heidbüchel et al., 2013; Hrachowitz et al., 2009a, 2009b, 2010; van der Velde et al., 2012).

We used the streamflow median travel time (MdTT) in our analysis (Figures 8 and 9), which is less sensitive to the uncertainties induced by old water fractions (see section 4.1). The MdTT ranged from 0.08 to 3.9 years during the 2001–2003 period (Figure 9) with an average (flow-weighted) value of 0.28 years. Klaus et al.

(2015) reported an average MdTT of 0.9 years over the same period. One reason for this difference relates to the way tracer data is used in each approach. The method of Klaus et al. (2015) gave more weight to the base flow samples to constrain simulations than our approach. These samples are associated with longer travel times. Our approach was able to better capture short-term variations during events that commonly have much younger age compositions than base flow periods. Another reason for this difference in the MdTT could be that we distinguished two main sources of streamflow (i.e., reservoirs) with drastically different TTDs. The most active reservoir was the one simulating the contributions of soil water from the hillslopes, with a high turnover rate. This reservoir provided mostly younger water (ages mostly below 1 year), especially during rainfall-runoff events (Figure 9) and gave the average MdTT a rather low value of 0.28 years. This is consistent with the estimated average MdTT of 0.25 years in the WS10 experimental hillslope (McGuire et al., 2007; van Verseveld et al., 2017). It is also consistent with the conclusion that soil depth (along with climate, as explained above) acts as a control on the MTT in WS10 (Sayama & McDonnell, 2009), which was also found at other sites (Capell et al., 2012; Heidbüchel et al., 2013; Hrachowitz et al., 2009b, 2010). In contrast to the shallow reservoir, the groundwater reservoir in this study had a low turnover rate. The variations of modeled groundwater storage were only around 5% over 1 year, consistent with the near absence of groundwater level changes in some wells in WS10 (Gabrielli et al., 2012). The groundwater reservoir provided mostly older water fractions (ages well above 1 year) to the stream (Figure 9). These groundwater contributions seem to be water that has flowed through tortuous pathways in the bedrock (Gabrielli et al., 2012). Most streamflow is derived from precipitation that fell a few months earlier, but the comparatively small volumetric contributions of water that is several years old (turquoise and red water age fractions in Figure 9) can substantially raise the average MdTT and especially the average MTT in WS10, as suggested by Gabrielli et al. (2012). Thus, the strong seasonality of streamflow travel times in WS10 is the result of seasonal hillslope contributions added to comparatively constant groundwater contributions. The hillslope connection and disconnection were driven by the precipitation regime.

Deep seepage loss was identified in WS10 and the surrounding catchments WS01, WS02, and WS03 (Gabrielli et al., 2012; Graham et al., 2010; Waichler et al., 2005). In our model conceptualization, this water was lost by ET active only in the shallow storage, which contains mostly younger water (ages < 1 year). This means that potentially more young water left the catchment model via ET than in reality, whereas the model should instead lose old groundwater via deep seepage. This may result in a bias toward older ages in the model compared to reality. Yet, Waichler et al. (2005) suggested that ET estimates in the lower part of the Lookout Creek at HJA are too low to close the water balance and need to be adjusted to account for the evaporation of the precipitation intercepted by humus and wood logs. More work in WS10 is needed to understand what water evaporates from the canopy and the soils, what water plants take up and eventually transpire (Barnard et al., 2010; Bond et al., 2002; Brooks et al., 2010), and how this may impact streamflow TTDs.

Our simulations with a conceptual model yielded streamflow travel time dynamics that were consistent with the previous understanding of how water ages are mobilized from storage in WS10 (Klaus et al., 2015; McGuire & McDonnell, 2010). This understanding was summarized in a perceptual model of the catchment (McGuire & McDonnell, 2010) consisting of three water age reservoirs: (1) event water (1–2 days old), (2) shallow reservoir (10–25 days old), and (3) deep reservoir (1–2 years old) associated with flow paths in (1) preferential networks, (2) hillslope soils, and (3) bedrock. Here we went beyond this perception, by showing that the relative contributions of these age reservoirs are highly time-variant and can be represented by contrasting streamflow SAS functions for the dry and wet seasons (Figure 6) in agreement with ISE (Figure 7). However, the ISE may not apply during transition periods, since different and competing transport processes create a hysteretic catchment response (Figure 8, McGuire et al., 2010). Hysteresis in storage-travel time response was also observed in three Scottish catchments (Hrachowitz et al., 2013). Hysteresis in catchment response indicates that significant changes occur in the source of the water mobilized to generate streamflow. This may be important to explain the rapid chemical response of catchments during runoff events in contrast with the relative absence of response in conservative tracers (Godsey et al., 2010; Kirchner, 2003). The transport processes influencing the WS10 response during wet-up periods could on the one hand be the redistribution of soil water from wetter to drier parts. On the other hand, preferential flow takes place in the unsaturated zone (McGuire et al., 2007, 2010) and in fractures below the soil-bedrock interface (Gabrielli et al., 2012), potentially acting as bypass mechanisms. During the spring dry-out, a generally

upward movement of the water, due to plant water uptake and evaporation, competes with downward unsaturated flow in soils. Conceptualizing the mixing of soil water at a smaller scale (e.g., pore scale) as in McGuire et al. (2007) and van Verseveld et al. (2017) to understand catchment scale transport effects (represented by SAS functions) paves the way for future research in WS10.

5. Conclusions

Our catchment conceptual model, developed based on experimental observations of water flow paths in WS10 (McGuire & McDonnell, 2010), was successful in modeling streamflow and ^{18}O transport. It allowed us to track water ages in catchment storage and outflows, and derive time-varying RTDs, and streamflow TTDs and SAS functions by solving the Master Equation. The streamflow SAS functions showed that the ISE dominates the age selection patterns in WS10 where the Mediterranean climate is highly seasonal. The catchment preferentially releases younger water in the winter after wetting up in late fall, while older water is preferentially released during dryer periods in the summer. The pronounced seasonality of streamflow travel times in WS10 is related to seasonal contributions of younger water from the hillslopes during wet periods. The streamflow SAS functions were a consistent lumped description of this mobilization of water from catchment storage, supported by the previous experimental and modeling work in WS10. During transition periods from dry states to wet states and vice versa, strong storage variations caused by the marked climate seasonality caused deviations from the ISE. These deviations occurred when changes in catchment storage were not linearly related to changes in streamflow SAS functions. These deviations also showed a DSE-like behavior over short periods of time. During transition periods, the catchment response was likely influenced by preferential flow and soil water redistribution caused by the drying effects of evapotranspiration. The streamflow SAS functions and travel time dynamics furthermore revealed that storage-travel time hysteresis exists in WS10. Overall, these findings suggest that future work with SAS functions needs to consider time variance and hysteresis in the relationships between catchment storage and water ages for catchments exposed to seasonal climates. The modeling results in this study also suggest that more work is needed in characterizing the soil water interactions in WS10. Such interactions could be implemented in lumped modeling approaches, for instance by using mixing coefficients or different SAS functions than in our study.

Acknowledgments
We gratefully acknowledge funding for this work, provided by the Luxembourg National Research Fund (FNR) in the framework of the STORE-AGE project (FNR/CORE/C14/SR/8353440/STORE-AGE). Precipitation, discharge, air temperature, and GIS data were provided by the HJ Andrews Experimental Forest and Long Term Ecological Research program, administered cooperatively by the USDA Forest Service Pacific Northwest Research Station, Oregon State University, and the Willamette National Forest. This material is based upon work supported by the National Science Foundation under Grant No. DEB-1440409. The data is freely available by contacting the corresponding author by email, and from the H. J. Andrews Experimental Forest research program (http://andrewsforest.oregonstate.edu/). We would like to thank Fabrizio Fenicia for providing the MRCtool MATLAB script, and Laurent Pfister for his constructive comments on the manuscript. Finally, we would like to thank the reviewer Markus Hrachowitz, one anonymous reviewer, and the editor for their helpful, critical, and supportive comments that helped us improve the manuscript.

References

Barnard, H. R., Graham, C. B., Van Verseveld, W. J., Brooks, J. R., Bond, B. J., & McDonnell, J. J. (2010). Mechanistic assessment of hillslope transpiration controls of diel subsurface flow: A steady-state irrigation approach. *Ecohydrology*, *3*(2), 133–142. https://doi.org/10.1002/eco.114

Benettin, P., Bailey, S. W., Campbell, J. L., Green, M. B., Rinaldo, A., Likens, G. E., et al. (2015a). Linking water age and solute dynamics in streamflow at the Hubbard Brook Experimental Forest, NH, USA. *Water Resources Research*, *51*, 9256–9272. https://doi.org/10.1002/2015WR017552

Benettin, P., Kirchner, J. W., Rinaldo, A., & Botter, G. (2015b). Modeling chloride transport using travel time distributions at Plynlimon, Wales. *Water Resources Research*, *51*, 3259–3276. https://doi.org/10.1002/2014WR016600

Benettin, P., Rinaldo, A., & Botter, G. (2015c). Tracking residence times in hydrological systems: Forward and backward formulations. *Hydrological Processes*, *29*(25), 5203–5213. https://doi.org/10.1002/hyp.10513

Benettin, P., Soulsby, C., Birkel, C., Tetzlaff, D., Botter, G., & Rinaldo, A. (2017). Using SAS functions and high-resolution isotope data to unravel travel time distributions in headwater catchments. *Water Resources Research*, *53*, 1864–1878. https://doi.org/10.1002/2016WR020117

Birkel, C., Dunn, S. M., Tetzlaff, D., & Soulsby, C. (2010a). Assessing the value of high-resolution isotope tracer data in the stepwise development of a lumped conceptual rainfall–runoff model. *Hydrological Processes*, *24*(16), 2335–2348. https://doi.org/10.1002/hyp.7763

Birkel, C., & Soulsby, C. (2016). Linking tracers, water age and conceptual models to identify dominant runoff processes in a sparsely monitored humid tropical catchment. *Hydrological Processes*, *30*(24), 4477–4493. https://doi.org/10.1002/hyp.10941

Birkel, C., Soulsby, C., & Tetzlaff, D. (2011a). Modelling catchment-scale water storage dynamics: Reconciling dynamic storage with tracer-inferred passive storage. *Hydrological Processes*, *25*(25), 3924–3936. https://doi.org/10.1002/hyp.8201

Birkel, C., Soulsby, C., & Tetzlaff, D. (2015). Conceptual modelling to assess how the interplay of hydrological connectivity, catchment storage and tracer dynamics controls nonstationary water age estimates. *Hydrological Processes*, *29*(13), 2956–2969. https://doi.org/10.1002/hyp.10414

Birkel, C., Tetzlaff, D., Dunn, S. M., & Soulsby, C. (2010b). Towards a simple dynamic process conceptualization in rainfall-runoff models using multi-criteria calibration and tracers in temperate, upland catchments. *Hydrological Processes*, *24*(3), 260–275. https://doi.org/10.1002/hyp.7478

Birkel, C., Tetzlaff, D., Dunn, S. M., & Soulsby, C. (2011b). Using lumped conceptual rainfall-runoff models to simulate daily isotope variability with fractionation in a nested mesoscale catchment. *Advances in Water Resources*, *34*(3), 383–394. https://doi.org/10.1016/j.advwatres.2010.12.006

Bond, B. J., Jones, J. A., Moore, G., Phillips, N., Post, D., & McDonnell, J. J. (2002). The zone of vegetation influence on baseflow revealed by diel patterns of streamflow and vegetation water use in a headwater basin. *Hydrological Processes*, *16*(8), 1671–1677. https://doi.org/10.1002/hyp.5022

Botter, G. (2012). Catchment mixing processes and travel time distributions. *Water Resources Research*, *48*, W05545. https://doi.org/10.1029/2011WR011160

Botter, G., Bertuzzo, E., & Rinaldo, A. (2010). Transport in the hydrologic response: Travel time distributions, soil moisture dynamics, and the old water paradox. *Water Resources Research*, *46*, W03514. https://doi.org/10.1029/2009WR008371

Botter, G., Bertuzzo, E., & Rinaldo, A. (2011). Catchment residence and travel time distributions: The master equation. *Geophysical Research Letters*, *38*, L11403. https://doi.org/10.1029/2011GL047666

Brooks, J. R., Barnard, H., Coulombe, R., & McDonnell, J. J. (2010). Ecohydrologic separation of water between trees and streams in a Mediterranean climate. *Nature Geoscience*, *3*, 100–104. https://doi.org/10.1038/ngeo722

Capell, R., Tetzlaff, D., Hartley, A. J., & Soulsby, C. (2012). Linking metrics of hydrological function and transit times to landscape controls in a heterogeneous mesoscale catchment. *Hydrological Processes*, *26*(3), 405–420. https://doi.org/10.1002/hyp.8139

Criss, R. E., & Winston, W. E. (2008). Do Nash values have value? Discussion and alternate proposals. *Hydrological Processes*, *22*(14), 2723–2725. https://doi.org/10.1002/hyp.7072

Danesh-Yazdi, M., Klaus, J., Condon, L. E., & Maxwell, R. M. (2018). Bridging the gap between numerical solutions of travel time distributions and analytical storage selection functions. *Hydrological Processes*, *32*, 1063–1076. https://doi.org/10.1002/hyp.11481

Dunn, S. M., Bacon, J. R., Soulsby, C., Tetzlaff, D., Stutter, M. I., Waldron, S., et al. (2008). Interpretation of homogeneity in $\delta^{18}O$ signatures of stream water in a nested sub-catchment system in north-east Scotland. *Hydrological Processes*, *22*(24), 4767–4782. https://doi.org/10.1002/hyp.7088

Dyrness, C. T. (1969). *Hydrologic properties of soils on three small watersheds in the western Cascades of Oregon* (Res. Note PNW-111). Portland, OR: Pacific Northwest Forest and Range Experiment Station, Forest Service, U.S. Department of Agriculture.

Fenicia, F., Kavetski, D., Savenije, H. H. G., & Pfister, L. (2016). From spatially variable streamflow to distributed hydrological models: Analysis of key modeling decisions. *Water Resources Research*, *52*, 954–989. https://doi.org/10.1002/2015WR017398

Fenicia, F., Savenije, H. H. G., Matgen, P., & Pfister, L. (2006). Is the groundwater reservoir linear? Learning from data in hydrological modelling. *Hydrology and Earth System Sciences*, *10*(1), 139–150. https://doi.org/10.5194/hess-10-139-2006

Fenicia, F., Wrede, S., Kavetski, D., Pfister, L., Hoffmann, L., Savenije, H. H. G., et al. (2010). Assessing the impact of mixing assumptions on the estimation of streamwater mean residence time. *Hydrological Processes*, *24*(12), 1730–1741. https://doi.org/10.1002/hyp.7595

Gabrielli, C. P., McDonnell, J. J., & Jarvis, W. T. (2012). The role of bedrock groundwater in rainfall-runoff response at hillslope and catchment scales. *Journal of Hydrology*, *450–451*, 117–133. https://doi.org/10.1016/j.jhydrol.2012.05.023

Godsey, S. E., Aas, W., Clair, T. A., de Wit, H. A., Fernandez, I. J., Kahl, J. S., et al. (2010). Generality of fractal 1/f scaling in catchment tracer time series, and its implications for catchment travel time distributions. *Hydrological Processes*, *24*(12), 1660–1671. https://doi.org/10.1002/hyp.7677

Graham, C. B., van Verseveld, W., Barnard, H., & McDonnell, J. J. (2010). Estimating the deep seepage component of the hillslope and catchment water balance within a measurement uncertainty framework. *Hydrological Processes*, *24*(25), 3631–3647. https://doi.org/10.1002/hyp.7788

Greenland, D. (1994). The Pacific Northwest regional context of the climate of the H. J. Andrews experimental forest long-term ecological research site. *Northwest Science*, *69*, 81–96.

Haraldsson, H., & Sverdrup, H. (2013). Finding simplicity in complexity in biogeochemical modelling. In J. Wainwright & M. Mulligan (Eds.), *Environmental modelling: Finding simplicity in complexity* (Chap. 17, pp. 277–289). Chichester, UK: Wiley. https://doi.org/10.1002/9781118351475.ch17

Harman, C. J. (2015). Time-variable transit time distributions and transport: Theory and application to storage-dependent transport of chloride in a watershed. *Water Resources Research*, *51*, 1–30. https://doi.org/10.1002/2014WR015707

Harr, R. D. (1977). Water flux in soil and subsoil on a steep forested slope. *Journal of Hydrology*, *33*(1), 37–58. https://doi.org/10.1016/0022-1694(77)90097-X

Harr, R. D., & McCorison, F. M. (1979). Initial effects of clearcut logging on size and timing of peak flows in a small watershed in western Oregon. *Water Resources Research*, *15*(1), 90–94. https://doi.org/10.1029/WR015i001p00090

Heidbüchel, I., Troch, P. A., & Lyon, S. W. (2013). Separating physical and meteorological controls of variable transit times in zero-order catchments. *Water Resources Research*, *49*, 7644–7657. https://doi.org/10.1002/2012WR013149

Heidbüchel, I., Troch, P. A., Lyon, S. W., & Weiler, M. (2012). The master transit time distribution of variable flow systems. *Water Resources Research*, *48*, W06520. https://doi.org/10.1029/2011WR011293

Hrachowitz, M., Benettin, P., van Breukelen, B. M., Fovet, O., Howden, N. J. K., Ruiz, L., et al. (2016). Transit times—The link between hydrology and water quality at the catchment scale. *Wiley Interdisciplinary Reviews: Water*, *3*(5), 629–657. https://doi.org/10.1002/wat2.1155

Hrachowitz, M., Fovet, O., Ruiz, L., & Savenije, H. H. G. (2015). Transit time distributions, legacy contamination and variability in biogeochemical 1/fα scaling: How are hydrological response dynamics linked to water quality at the catchment scale?. *Hydrological Processes*, *29*(25), 5241–5256. https://doi.org/10.1002/hyp.10546

Hrachowitz, M., Savenije, H., Bogaard, T. A., Tetzlaff, D., & Soulsby, C. (2013). What can flux tracking teach us about water age distribution patterns and their temporal dynamics?. *Hydrology and Earth System Sciences*, *17*(2), 533–564. https://doi.org/10.5194/hess-17-533-2013

Hrachowitz, M., Soulsby, C., Tetzlaff, D., Dawson, J. J. C., Dunn, S. M., & Malcolm, I. A. (2009a). Using long-term data sets to understand transit times in contrasting headwater catchments. *Journal of Hydrology*, *367*(3), 237–248. https://doi.org/10.1016/j.jhydrol.2009.01.001

Hrachowitz, M., Soulsby, C., Tetzlaff, D., Dawson, J. J. C., & Malcolm, I. A. (2009b). Regionalization of transit time estimates in montane catchments by integrating landscape controls. *Water Resources Research*, *45*, W05421. https://doi.org/10.1029/2008WR007496

Hrachowitz, M., Soulsby, C., Tetzlaff, D., & Malcolm, I. A. (2011). Sensitivity of mean transit time estimates to model conditioning and data availability. *Hydrological Processes*, *25*(6), 980–990. https://doi.org/10.1002/hyp.7922

Hrachowitz, M., Soulsby, C., Tetzlaff, D., Malcolm, I. A., & Schoups, G. (2010). Gamma distribution models for transit time estimation in catchments: Physical interpretation of parameters and implications for time-variant transit time assessment. *Water Resources Research*, *46*, W10536. https://doi.org/10.1029/2010WR009148

Jasechko, S., Kirchner, J. W., Welker, J. M., & McDonnell, J. J. (2016). Substantial proportion of global streamflow less than three months old. *Nature Geoscience*, *9*, 126–129. https://doi.org/10.1038/ngeo2636

Kim, M., Pangle, L. A., Cardoso, C., Lora, M., Volkmann, T. H. M., Wang, Y., et al. (2016). Transit time distributions and StorAge Selection functions in a sloping soil lysimeter with time-varying flow paths: Direct observation of internal and external transport variability. *Water Resources Research*, *52*, 7105–7129. https://doi.org/10.1002/2016WR018620

Kirchner, J. W. (2003). A double paradox in catchment hydrology and geochemistry. *Hydrological Processes*, *17*(4), 871–874. https://doi.org/10.1002/hyp.5108

Kirchner, J. W. (2006). Getting the right answers for the right reasons: Linking measurements, analyses, and models to advance the science of hydrology. *Water Resources Research*, *42*, W03S04. https://doi.org/10.1029/2005WR004362

Kirchner, J. W. (2016). Aggregation in environmental systems—Part 2: Catchment mean transit times and young water fractions under hydrologic nonstationarity. *Hydrology and Earth System Sciences*, *20*(1), 299–328. https://doi.org/10.5194/hess-20-299-2016

Kirchner, J. W., Feng, X., & Neal, C. (2000). Fractal stream chemistry and its implications for contaminant transport in catchments. *Nature*, *403*, 524–527. https://doi.org/10.1038/35000537

Kirchner, J. W., Feng, X., Neal, C., & Robson, A. J. (2004). The fine structure of water-quality dynamics: The (high-frequency) wave of the future. *Hydrological Processes*, *18*(7), 1353–1359. https://doi.org/10.1002/hyp.5537

Klaus, J., Chun, K. P., McGuire, K. J., & McDonnell, J. J. (2015). Temporal dynamics of catchment transit times from stable isotope data. *Water Resources Research*, *51*, 4208–4223. https://doi.org/10.1002/2014WR016247

Klaus, J., Zehe, E., Elsner, M., Külls, C., & McDonnell, J. J. (2013). Macropore flow of old water revisited: Experimental insights from a tile-drained hillslope. *Hydrology and Earth System Sciences*, *17*(1), 103–118. https://doi.org/10.5194/hess-17-103-2013

Lamb, R., & Beven, K. (1997). Using interactive recession curve analysis to specify a general catchment storage model. *Hydrology and Earth System Sciences*, *1*(1), 101–113. https://doi.org/10.5194/hess-1-101-1997

Legout, C., Molenat, J., Aquilina, L., Gascuel-Odoux, C., Faucheux, M., Fauvel, Y., et al. (2007). Solute transfer in the unsaturated zone-groundwater continuum of a headwater catchment. *Journal of Hydrology*, *332*(3–4), 427–441. https://doi.org/10.1016/j.jhydrol.2006.07.017

Maher, K. (2010). The dependence of chemical weathering rates on fluid residence time. *Earth and Planetary Science Letters*, *294*(1–2), 101–110. https://doi.org/10.1016/j.epsl.2010.03.010

Maher, K. (2011). The role of fluid residence time and topographic scales in determining chemical fluxes from landscapes. *Earth and Planetary Science Letters*, *312*(1–2), 48–58. https://doi.org/10.1016/j.epsl.2011.09.040

McDonnell, J. J., & Beven, K. (2014). Debates—The future of hydrological sciences: A (common) path forward? A call to action aimed at understanding velocities, celerities and residence time distributions of the headwater hydrograph. *Water Resources Research*, *50*, 5342–5350. https://doi.org/10.1002/2013WR015141

McGuire, K. J., & McDonnell, J. J. (2006). A review and evaluation of catchment transit time modeling. *Journal of Hydrology*, *330*(3–4), 543–563. https://doi.org/10.1016/j.jhydrol.2006.04.020

McGuire, K. J., & McDonnell, J. J. (2010). Hydrological connectivity of hillslopes and streams: Characteristic time scales and nonlinearities. *Water Resources Research*, *46*, W10543. https://doi.org/10.1029/2010WR009341

McGuire, K. J., McDonnell, J. J., Weiler, M., Kendall, C., McGlynn, B. L., Welker, J. M., et al. (2005). The role of topography on catchment-scale water residence time. *Water Resources Research*, *41*, W05002. https://doi.org/10.1029/2004WR003657

McGuire, K. J., Weiler, M., & McDonnell, J. J. (2007). Integrating tracer experiments with modeling to assess runoff processes and water transit times. *Advances in Water Resources*, *30*(4), 824–837. https://doi.org/10.1016/j.advwatres.2006.07.004

McMillan, H., Tetzlaff, D., Clark, M., & Soulsby, C. (2012). Do time-variable tracers aid the evaluation of hydrological model structure? A multimodel approach. *Water Resources Research*, *48*, W05501. https://doi.org/10.1029/2011WR011688

Monteith, J. L. (1965). Evaporation and environment. *Symposia of the Society for Experimental Biology*, *19*, 205–234. https://doi.org/10.1002/qj.49710745102

Nash, J. E., & Sutcliffe, J. V. (1970). River flow forecasting through conceptual models. Part I—A discussion of principles. *Journal of Hydrology*, *10*(3), 282–290. https://doi.org/10.1016/0022-1694(70)90255-6

Nippgen, F., McGlynn, B. L., & Emanuel, R. E. (2015). The spatial and temporal evolution of contributing areas. *Water Resources Research*, *51*, 4550–4573. https://doi.org/10.1002/2014WR016719

Page, T., Beven, K. J., Freer, J., & Neal, C. (2007). Modelling the chloride signal at Plynlimon, Wales, using a modified dynamic TOPMODEL incorporating conservative chemical mixing (with uncertainty). *Hydrological Processes*, *21*(3), 292–307. https://doi.org/10.1002/hyp.6186

Pangle, L. A., Kim, M., Cardoso, C., Lora, M., Meira Neto, A. A., Volkmann, T. H. M., et al. (2017). The mechanistic basis for storage-dependent age distributions of water discharged from an experimental hillslope. *Water Resources Research*, *53*, 2733–2754. https://doi.org/10.1002/2016WR019901

Rinaldo, A., Benettin, P., Harman, C. J., Hrachowitz, M., McGuire, K. J., van der Velde, Y., et al. (2015). Storage selection functions: A coherent framework for quantifying how catchments store and release water and solutes. *Water Resources Research*, *51*, 4840–4847. https://doi.org/10.1002/2015WR017273

Rinaldo, A., Beven, K. J., Bertuzzo, E., Nicotina, L., Davies, J., Fiori, A., et al. (2011). Catchment travel time distributions and water flow in soils. *Water Resources Research*, *47*, W07537. https://doi.org/10.1029/2011WR010478

Rinaldo, A., & Marani, A. (1987). Basin scale model of solute transport. *Water Resources Research*, *23*(11), 2107–2118.

Rothacher, J. S. (2016). *Stream discharge in gaged watersheds at the Andrews Experimental Forest, 1949 to present. Environmental Data Initiative*. https://doi.org/10.6073/pasta/ce70a42e1f637cd430d7b0fb64faefb4

Rothacher, J., Fredricksen, R. L., & Dyrness, C. T. (1967). *Hydrologic and related characteristics of three small watersheds in the Oregon Cascades*. Portland, OR: U.S. Department of Agriculture, Forest Service, Pacific Northwest Forest and Range Experiment Station.

Sayama, T., & McDonnell, J. J. (2009). A new time-space accounting scheme to predict stream water residence time and hydrograph source components at the watershed scale. *Water Resources Research*, *45*, W07401. https://doi.org/10.1029/2008WR007549

Scaini, A., Hissler, C., Fenicia, F., Juilleret, J., Iffly, J. F., Pfister, L., et al. (2017). Hillslope response to sprinkling and natural rainfall using velocity and celerity estimates in a slate-bedrock catchment. *Journal of Hydrology*, *558*, 366–379. https://doi.org/10.1016/j.jhydrol.2017.12.011

Segura, C., James, A. L., Lazatti, D., & Roulet, N. T. (2012). Scaling relationships for event water contributions and transit times in small-forested catchments in Eastern Quebec. *Water Resources Research*, *48*, W07502. https://doi.org/10.1029/2012WR011890

Sollins, P., & McCorison, F. M. (1981). Nitrogen and carbon solution chemistry of an old growth coniferous forest watershed before and after cutting. *Water Resources Research*, *17*(5), 1409–1418. https://doi.org/10.1029/WR017i005p01409

Soulsby, C., Birkel, C., Geris, J., Dick, J., Tunaley, C., & Tetzlaff, D. (2015a). Stream water age distributions controlled by storage dynamics and nonlinear hydrologic connectivity: Modeling with high-resolution isotope data. *Water Resources Research*, *51*, 7759–7776. https://doi.org/10.1002/2015WR017888

Soulsby, C., Birkel, C., Geris, J., & Tetzlaff, D. (2015b). Spatial aggregation of time-variant stream water ages in urbanizing catchments. *Hydrological Processes*, *29*(13), 3038–3050. https://doi.org/10.1002/hyp.10500

Stewart, M. K., Morgenstern, U., McDonnell, J. J., & Pfister, L. (2012). The 'hidden streamflow' challenge in catchment hydrology: A call to action for stream water transit time analysis. *Hydrological Processes*, *26*(13), 2061–2066. https://doi.org/10.1002/hyp.9262

Swanson, F. J., & James, M. E. (1975). *Geology and geomorphology of the H. J. Andrews Experimental Forest, western Cascades, Oregon* (Res. Pap. PNW-188). Portland, OR: Pacific Northwest Forest and Range Experiment Station, Forest Service, U.S. Department of Agriculture.

Tetzlaff, D., Seibert, J., McGuire, K. J., Laudon, H., Burns, D. A., Dunn, S. M., et al. (2009). How does landscape structure influence catchment transit time across different geomorphic provinces?. *Hydrological Processes*, *23*(6), 945–953. https://doi.org/10.1002/hyp.7240

Thornthwaite, C. W. (1948). An approach toward a rational classification of climate. *Geographical Review*, *38*(1), 55–94. https://doi.org/10.2307/210739

Vaché, K. B., & McDonnell, J. J. (2006). A process-based rejectionist framework for evaluating catchment runoff model structure. *Water Resources Research*, *42*, W02409. https://doi.org/10.1029/2005WR004247

van Verseveld, W. J., Barnard, H. R., Graham, C. B., McDonnell, J. J., Brooks, J. R., & Weiler, M. (2017). A sprinkling experiment to quantify celerity-velocity differences at the hillslope scale. *Hydrology and Earth System Sciences*, *21*, 5891–5910. https://doi.org/10.5194/hess-21-5891-2017

van der Velde, Y., Heidbüchel, I., Lyon, S. W., Nyberg, L., Rodhe, A., Bishop, K., et al. (2015). Consequences of mixing assumptions for time-variable travel time distributions. *Hydrological Processes*, *29*(16), 3460–3474. https://doi.org/10.1002/hyp.10372

van der Velde, Y., Torfs, P. J. J. F., van der Zee, S. E. A. T. M., & Uijlenhoet, R. (2012). Quantifying catchment-scale mixing and its effect on time-varying travel time distributions. *Water Resources Research*, *48*, W06536. https://doi.org/10.1029/2011WR011310

Waichler, S. R., Wemple, B. C., & Wigmosta, M. S. (2005). Simulation of water balance and forest treatment effects at the H.J. Andrews Experimental Forest. *Hydrological Processes*, *19*(16), 3177–3199. https://doi.org/10.1002/hyp.5841

Wilusz, D. C., Harman, C. J., & Ball, W. P. (2017). Sensitivity of catchment transit times to rainfall variability under present and future climates. *Water Resources Research*, *53*, 10231–10256. https://doi.org/10.1002/2017WR020894

Zehe, E., Elsenbeer, H., Lindenmaier, F., Schulz, K., & Blöschl, G. (2007). Patterns of predictability in hydrological threshold systems. *Water Resources Research*, *43*, W07434. https://doi.org/10.1029/2006WR005589